AFRL-ML-TY-TR-2006-4540

BLAST RETROFIT DESIGN OF CMU WALLS USING POLYMER SHEETS

Silas James Fitzmaurice and Hani Salim
University of Missouri - Columbia
Department of Civil and Environmental Engineering
E2509 Engineering Building East
Columbia, MO 65211-2200

Robert J. Dinan and Elizabeth Trawinski
Air Force Research Laboratory
139 Barnes Drive, Suite 2
Tyndall AFB, FL 32403-5323

Interim Report, May 2006

Air Force Research Laboratory
Materials and Manufacturing Directorate
Airbase Technologies Division
139 Barnes Drive, Suite 2
Tyndall AFB, FL 32403-5323

REPORT DOCUMENTATION PAGE

Form Approved
OMB No. 0704-0188

PLEASE DO NOT RETURN YOUR FORM TO THE ABOVE ADDRESS.

1. REPORT DATE *(DD-MM-YYYY)*	2. REPORT TYPE	3. DATES COVERED *(From - To)*
01-05-2006	Interim Technical Report	01-08-2005 -- 01-05-2006

4. TITLE AND SUBTITLE

Blast Retrofit Design of CMU Walls Using Polymer Sheets

5a. CONTRACT NUMBER

F08637-03-C-6006

5b. GRANT NUMBER

5c. PROGRAM ELEMENT NUMBER

63112F

6. AUTHOR(S)

Fitzmaurice, Silas J.; Salim, Hani A.; Dinan, Robert J.

5d. PROJECT NUMBER

4918

5e. TASK NUMBER

C10B

5f. WORK UNIT NUMBER

4918C10B

7. PERFORMING ORGANIZATION NAME(S) AND ADDRESS(ES)

University of Missouri - Columbia
Department of Civil and Environmental Engineering
E2509 Engineering Building East
Columbia, MO 65211-2200

8. PERFORMING ORGANIZATION REPORT NUMBER

9. SPONSORING/MONITORING AGENCY NAME(S) AND ADDRESS(ES)

Air Force Research Laboratory
Materials and Manufacturing Directorate
139 Barnes Drive, Suite 2
Tyndall AFB, FL 32403-5323

10. SPONSOR/MONITOR'S ACRONYM(S)

AFRL/MLQF

11. SPONSOR/MONITOR'S REPORT NUMBER(S)

AFRL-ML-TY-TR-2006-4540

12. DISTRIBUTION/AVAILABILITY STATEMENT

DISTRIBUTION STATEMENT A: Approved for public release; distribution unlimited.

13. SUPPLEMENTARY NOTES

Technical contact: Dr. Robert J. Dinan, AFRL/MLQF, 850-283-3605. Report contains color images.
AFRL/MLQ Public Affairs Case # 06-044.

14. ABSTRACT

The research presented in this thesis details the development of analytical modeling and experimental evaluation of CMU-polymer walls to blast loading. Polymer sheets were analyzed as a method for retrofit design. This research was done to ascertain the strength, ductility, response to static pressure, investigate connection details, and develop an analytical model of the static resistance function. The analytical model developed for the static resistance was used in a SDOF model to dynamically model the polymer retrofit system. Three types of test were conducted at the coupon, connection, and component levels to verify the analytical model. Once the analytical model was verified, it was incorporated into the SDOF model. Additionally, field tests were conducted on three polymers, and results were compared to the predicted results.

15. SUBJECT TERMS

sheet polymers, concrete masonry unit, blast response, polymer reinforced, blast retrofit design, static resistance

16. SECURITY CLASSIFICATION OF:			17. LIMITATION OF ABSTRACT	18. NUMBER OF PAGES	19a. NAME OF RESPONSIBLE PERSON
a. REPORT	b. ABSTRACT	c. THIS PAGE			Elizabeth Trawinski
U	U	U	UU	103	19b. TELEPHONE NUMBER *(Include area code)*

NOTICE

Using Government drawings, specifications, or other data included in this document for any purpose other than Government procurement does not in any way obligate the U.S. Government. The fact that the Government formulated or supplied the drawings, specifications, or other data does not license the holder or any other person or corporation; or convey any rights or permission to manufacture, use, or sell any patented invention that may relate to them.

This technical report was reviewed and cleared for public release by the Air Force Research Laboratory Tyndall Site (AFRL/MLQ) Public Affairs Office (PAO) and is releasable to the National Technical Information Service (NTIS). Reference PAO Case Number: AFRL/MLQ-06-044.

This report is releasable to the National Technical Information Service (NTIS) where it will be available to the general public, including foreign nationals.

5285 Port Royal Road
Springfield VA 22161
Telephone (703) 487-4650, (703) 487-4639 (TDD for the hearing impaired)
e-mail: orders@ntis.fedworld.gov
http://www.ntis.gov/index.html

This technical report is approved for publication.

/s/
ELIZABETH TRAWINSKI, Capt, USAF
Work Unit Manager

/s/
JEREMY R. GILBERTSON, Capt, USAF
Acting Chief, Force Protection Branch

/s/
MICHAEL R. UPDIKE, Lt Col, USAF
Deputy Chief, Airbase Technologies Division

This report is published in the interest of scientific and technical information exchange and its publication does not constitute the Government's approval or disapproval of its ideas or findings.

ABSTRACT

The focus of this research was the analysis of polymer sheets as a method for retrofit design. Many materials have been tested for blast retrofit design but have shown their limitations. There are many advantages to polymer sheets. For example, the sheets are very thin and take up very little space, polymers have large amounts of energy absorption capabilities, and the installation process is quick and easy to perform in the field.

This research was done to ascertain the strength, ductility, response to static pressure, investigate connection details, and develop an analytical model of the static resistance function. The polymer retrofit system was modeled dynamically in a single-degree of freedom (SDOF) model, and the analytical model developed for the static resistance was used in the SDOF model. Additionally, three types of tests were conducted at the coupon, connection, and component levels to verify the analytical model. Once the analytical model was verified, it was incorporated into the SDOF model. Finally, field tests were conducted on three polymers, and results were compared to the predicted results made by this project. This report presents the analytical modeling and experimental evaluation of CMU-polymer wall systems subjected to blast loading.

TABLE OF CONTENTS

LIST OF FIGURES

LIST OF TABLES

CHAPTER 1 -- INTRODUCTION

1.1 General

Due to the increasing need for blast resistant structures, many retrofit systems have been developed to increase the energy absorption of typical infill concrete masonry unit (CMU) walls. CMU walls are chosen because they are commonly used in the field and easy to construct. Most CMU walls are designed for typical structural loads like dead loads, live loads, wind loads, and snow loads. Accordingly, they have very low resistances to blast loading and fail catastrophically under blast pressure producing hazardous projectiles that enter the structure. Blast loads are unlike any other type of load; they are short in duration and high in pressure. One important property of a blast is the reflected impulse. Generally, the reflected impulse governs the design and not the peak pressure (Stone and Engebretsen, 2001). Because the reflected impulse is the governing property, the retrofit material does not necessarily have to have high strength, but must be very ductile and have high energy absorption capabilities. Many steel retrofit systems have been investigated and proven to be effective, such as steel studs (Dinan, 2005) and steel sheathing (Kennedy, 2005). Also, many polymer retrofit systems have been evaluated and determined to be effective, such as spray-on and trowel-on polymers (Beckman, 2004 and Davidson, 2005) and fiber reinforced polymers (Albert, 2001). For this project, polymer sheets were evaluated as a method to enhance the ductility and energy absorption of an infill masonry wall system. Instead of spraying or troweling the polymer to the wall, the polymer is installed using long sheets that span the full length of the wall and anchored to the ceiling and floors using mechanical connections. To advance this technology and material for blast-retrofit of CMU walls, it is necessary to

develop an engineering design methodology and response prediction models under blast loads. Therefore, the objective of this research was to develop an analytical model to be used in a single-degree of freedom (SDOF) model which predicts the midspan deflection of a CMU wall and polymer system under blast loads.

1.2 Purpose and Scope

The purpose of this research was to develop the static resistance function of polymer sheets under uniform pressure. In order to develop the static resistance function, many tasks were performed. The first task was to analytically predict the response of the polymer sheets to uniform pressure. The second task was to perform experimental tests at three levels. The first test series was at the coupon level, which was needed in order to find the stress-strain relationship of the polymer sheets. Next, connection test series were performed to ensure that the polymer sheets would not fail at the connection which would inhibit the polymer to develop its full capacity. Then, component tests were conducted in order to experimentally verify the analytical resistance function developed. The third task was to develop a dynamic model using the experimental and analytical data to determine the suitability of the polymer to resist blast loading. The fourth task was to compare the model to field data collected from tests performed by the United States Air Force Research Laboratory (AFRL) at Tyndall Air Force Base (AFB), FL. Finally, the results were implemented into a PC-code, the Air Force Wall Analysis Code (AFWAC), to be used for future engineering design.

1.3 Approach

In an effort to predict the behavior of polymer sheets, an analytical model was developed. The analytical model, or static resistance function, predicted the pressure-deflection graph for the polymer sheets. The analytical model was then compared to the experimental data, obtained by using a 16-point loading tree simulating a uniform pressure loading.

Coupon tests on samples cut from polymer sheets were tested under uniaxial tension to failure using a constant head speed of 2 inches per minute. ASTM D638 standard was used to prepare and test the samples. The testing parameters for the connection tests were the two gage thicknesses of the polymer sheets, bolt spacing, and connection plate thicknesses. From the connection tests, an optimal combination of the parameters were found and used for the component tests. For the component tests, two gage thicknesses of the polymer sheet, the optimal connection plate thickness, and the optimal bolt spacing were used. Load-deflection response of the component tests were recorded and used to verify the analytical model developed. The load-deflection curves developed in these component tests were used to calculate the equivalent pressure-displacement response (Static Resistance Function) of the blast mitigation system, which was useful for predicting the dynamic response of the blast-retrofitted wall system.

CHAPTER 2 – LITERATURE REVIEW

2.1 General

Due to an increase in the number of bombing threats, significant research has been conducted in an effort to retrofit structures to resist blast loading. The idea behind the retrofit systems is that they are inexpensive, easy to install, and protect the occupants of the facilities. Several retrofit systems that have already been explored are the use of steel studs, steel sheets, fiber reinforced polymers, and trowel-on and spray-on polymers. Many papers and publications have been written on each of these retrofit systems.

2.2 Technical Background

To evaluate a blast retrofit design, it is crucial to understand the mechanics of a blast load and how a structure will react to the load. A blast loading comes from an explosion, which is defined as a rapid release of energy in the form of light, heat, sound, and a shockwave (Stone and Engebretsen, 2001). This shock wave released from the blast expands radially out from the source causing extremely large loading on the target structure. These targets, which are generally buildings, are typically only designed for wind load, which can cause pressures ranging in magnitude from 0.3 to 0.5 psi. However, blast loading can cause pressures typically ranging in magnitude from 30 to 50 psi, depending on the size of the explosive, distance from the target, and angle of incidence. A typical blast load is shown in Figure 2.1. From the figure, it can be seen that there is a positive and a negative phase. The positive phase of the blast loading has a duration of 15 ms. The negative phase, which typically reduces damage caused by the blast, is typically ignored. In this report, the effects of this region will be evaluated.

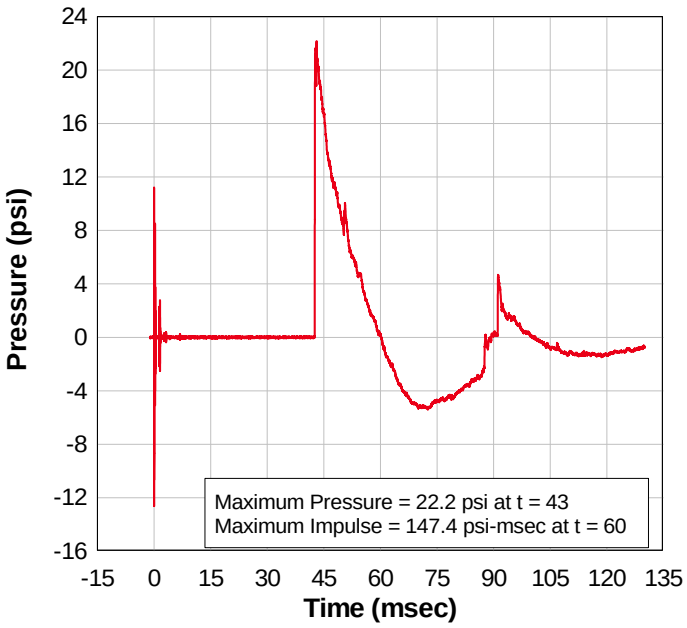

Figure 2.1 – Typical Blast Loading

Although blast loads have extremely high peak pressure, the duration of these pressures are very short, which is advantageous in the design. Typically, structures are designed for peak loading, but for blast-resistant structures, the duration is so short compared to the natural period that the blast impacts the structure and is gone before the structure responds significantly. This means the structure feels no peak pressure, but it feels the energy imparted by the blast. The reason is that the natural period of a concrete structure is typically in the range of 100 to 200 ms and a blast only lasts 15 ms. Instead of designing the structure for peak pressures, it is designed to withstand the energy of the blast. Additionally, typical structures are designed using the assumption that the members are linearly elastic whether they are actually in the elastic or plastic range. This keeps deflection limits low causing low energy-absorption. For blast design,

methodologies must allow the structure to undergo permanent plastic deformations to increase the energy absorption capabilities (Dinan, 2005).

2.3 Previous Blast Retrofit Research

Much research has been done retrofitting systems for blast loading. Specifically, retrofit of non-load bearing concrete masonry units (CMU) walls have been the main focus of such research. The reason for this focus is that these walls are frequently used in construction, and when introduced to blast loading, they tend to cause a great deal of fragmentation under low pressures (Davidson et al., 2005). The following is an overview of the work done for the design of blast-retrofitted structures.

One of the retrofit systems investigated was the use of steel sheathing for blast retrofit design done by Kennedy (2005). In this research, thin steel sheets of various parameters were tested and performance was evaluated for blast design. The parameters included gages of steel sheathing, bolt spacing of connections, welded or bolted connections, and thickness of the connection plate. A static resistance function was developed and implemented into a dynamic modeling system. The modeling system then, given blast loading parameters, predicted the behavior of the wall retrofit system. The research provided conclusive evidence that the steel sheathing system could adequately resist blast loading (Kennedy, 2005).

Additionally, extensive research has been conducted in using polymers for blast retrofit design. In December 2000, a team of researchers conducted three full-scale tests to determine the effectiveness of polymers to improve the blast resistance of unreinforced masonry walls. Some of the walls were reinforced with polymers and some were not, used as control walls to test the effectiveness of the polymers. The tests were designed to

(1) evaluate the elastomeric polymer application process; (2) measure deflections at critical wall locations; (3) measure internal and external pressures created by the blast; (4) determine the failure modes; and (5) assess the general effectiveness and level of protection provided by the elastomeric polymer retrofit (Davidson et al., 2004). The polymers used in these tests were spray-on polymers chosen based on stiffness, ductility, fire resistance, and cost. In each of the tests an explosive charge was placed a certain distance away from the reinforced and unreinforced structures. These parameters were not released by the research team due to the sensitive nature of the project. The tests concluded that the spray-on polymer retrofit approach for strengthening masonry wall systems against blast loads can be effective. However, these materials were deemed a poor choice due to high cost, difficulty adhering the material to the wall, and anchoring the material to the surrounding structure (Davidson et al., 2004).

Another paper by Davison (2005) discussed the damage and failure mechanisms observed from twelve polymer-reinforced masonry walls. The tests were to establish the limits of blast resistance effectiveness of polymer-reinforced masonry walls. The main observations of Davidson (2005) indicated that: (1) Thin elastomeric coating on the interior wall can eliminate secondary fragmentation and aid in preventing a collapse of the masonry wall; (2) A spray overlap of 6 in. of the polymer onto the surrounding structure provides enough strength to transfer loads from a blast to the structural frame to prevent collapse of a polymer-reinforced masonry wall; (3) Although an effective balance should be maintained between stiffness and elongation ability, the elongation capacity is more important for this purpose than having a high stiffness. Additionally, a better balance between stiffness, shear tearing resistance, strength, and strain capacity should

result in a more effective reinforcement; (4) Spray-on polymer used in the test bonded well to the masonry. However, this could cause concentrated strains at mortar joints and minimal strains to most of the polymer. An optimized balance between bond strength, strain energy absorption, and overlap strength may result in a more effective reinforcement system. Similar results were reported by Beckman (2005); (5) Front face shell fracture of the masonry of polymer-reinforced walls is common when the peak load is close to the loading capacity of the polymer-reinforced wall. This behavior should be further tested when considering the development of the static resistance function; (6) Significant arching effects were evident in some of the tests. Finite element results indicate that tight fit of the wall and the host frame is needed for significant arching stiffness to occur. Mortar in the joints provides freedom of movement that reduces arching effects; (7) A strong bond between the polymer and the wall was crucial in the effectiveness of the wall system. Without this, the material resulted in tearing at the connection of the polymer coating to the host structure and collapse of the wall. However, a catcher membrane approach offers the potential advantage of more-efficiently absorbing strain energy over the greater reinforcement volume, as well as the use of a wide range of more cost effective material (Beckman 2005 and Bechtold 2004); (8) Both finite element results and post-test analysis indicate that the upper-most mortar joints fracture in the early stages of flexure, resulting in relative displacement of the two courses of block causing high shear strains in the polymer. This shows the importance of shear tearing resistance in an external reinforcement product; (9) For the masonry structures considered in this study, the rate of strain in the polymer was significant, but not high. Finite element indicates a maximum strain rate below 100 s^{-1}; (10) For walls

with window or door openings, some effects were noted. A larger area of front face shell fracture, a tendency for tearing to initiate at the door or window frame, and additional breaching was observed. However, the overall effectiveness of the polymer remained high. Although the effectiveness of the polymer is very high, it should still be noted that there are still several problems. The polymers, when sprayed, emit toxic volatiles and require protective clothing. Additionally, the equipment used is expensive and can be difficult to operate (Davidson et al., 2005).

Based on the research conducted by Beckman (2005) and Bechtold (2004) on small-scale concrete beams retrofitted with polymer sheets, the blast resistance is mostly attributed to the increased energy-absorption capability of the polymer (Figures 2.2 and 2.3). The research also indicated that a weak bond or no bond between the polymer and concrete wall is needed to obtain desirable performance. A strong bond between the polymer and the wall could cause the polymer to tear prematurely due to large localized elongation at the location of the crack (Beckman, 2005). No bond can be achieved easily in the case of polymer sheets, whereas weak bonds can be achieved by painting the wall prior to spraying or toweling the polymer onto the CMU wall.

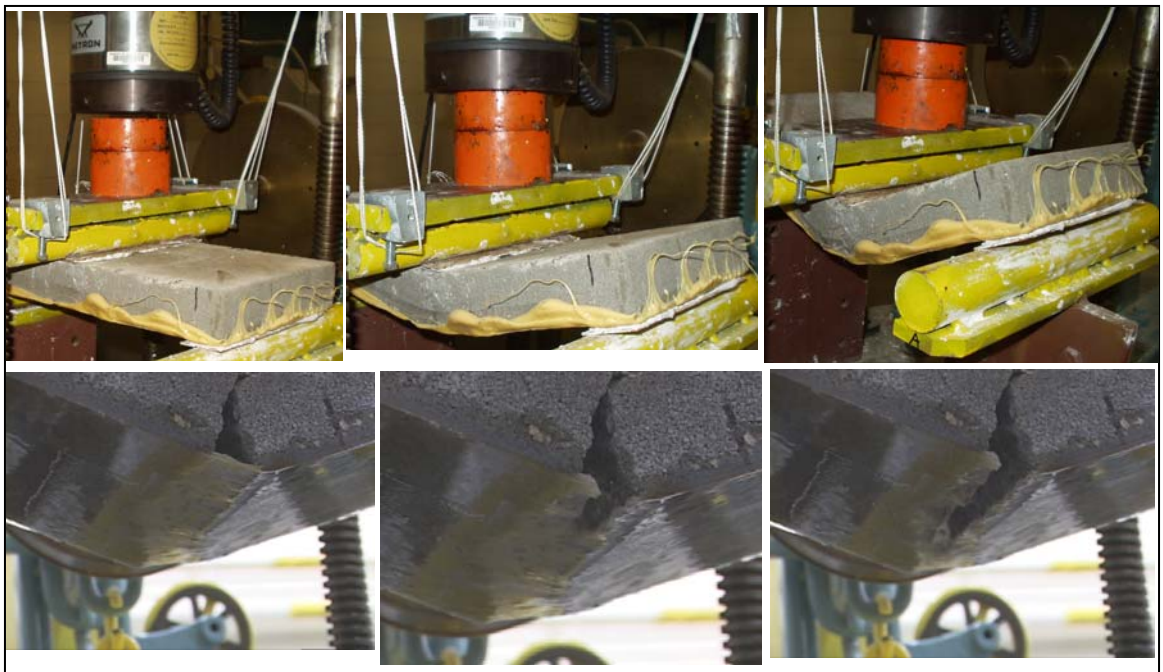

Figure 2.2 – Small-scale Testing of Polymer Retrofitted Concrete Beams. Weak bond allows polymer to stretch without tearing (top), whereas a strong bond causes polymer to tear at initial crack location in concrete (bottom).

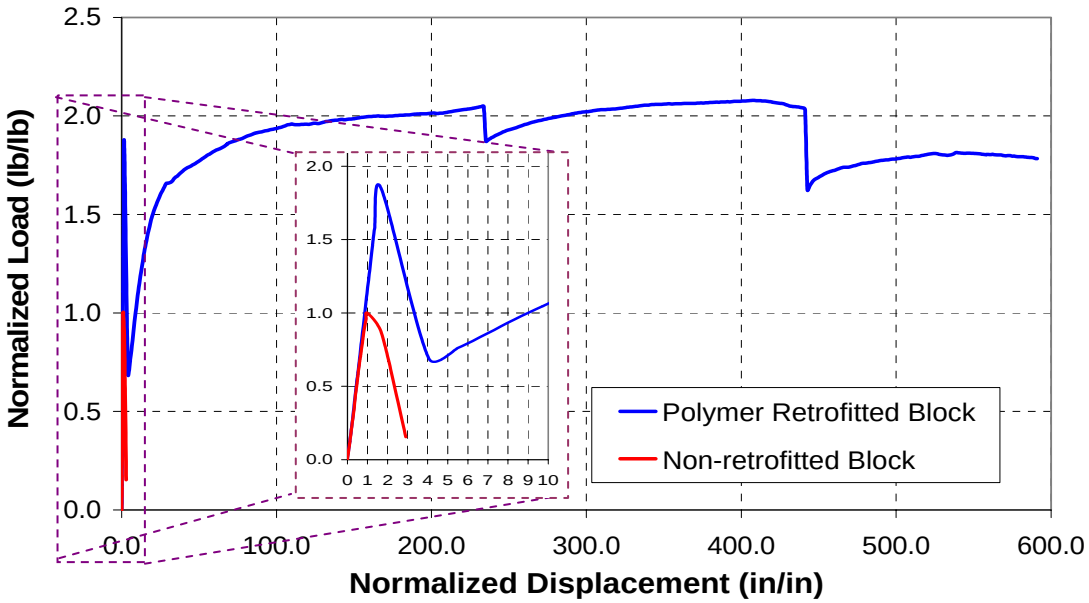

Figure 2.3 – Average Normalized Load vs. Displacement Curve of Concrete Samples. Graph is normalized with respect to peak response of non-retrofitted samples.

CHAPTER 3 – ANALYTICAL MODELING OF THE STATIC RESISTANCE FUNCTION OF POLYMER SHEETS

To derive the exact analytical model, four principle steps are followed to find pressure in terms of deflection. The first step is to assume a deformed shape of the polymer sheets under uniform loading (Figure 3.1). The deflected shape is assumed to be parabolic in nature (Lane, 2003). Once the deformed shape has been established, a free body diagram is made, and equilibrium is used to find a relationship between load and stress. Next, using the coupon data and the constitutive relation between stress and strain, a relationship is found between pressure and stress. Finally, a compatibility relationship between deflection and strain is analyzed, ultimately resulting in the desired relationship between pressure and deflection, the static resistance function. This process is outlined through the flow chart in Figure 3.2.

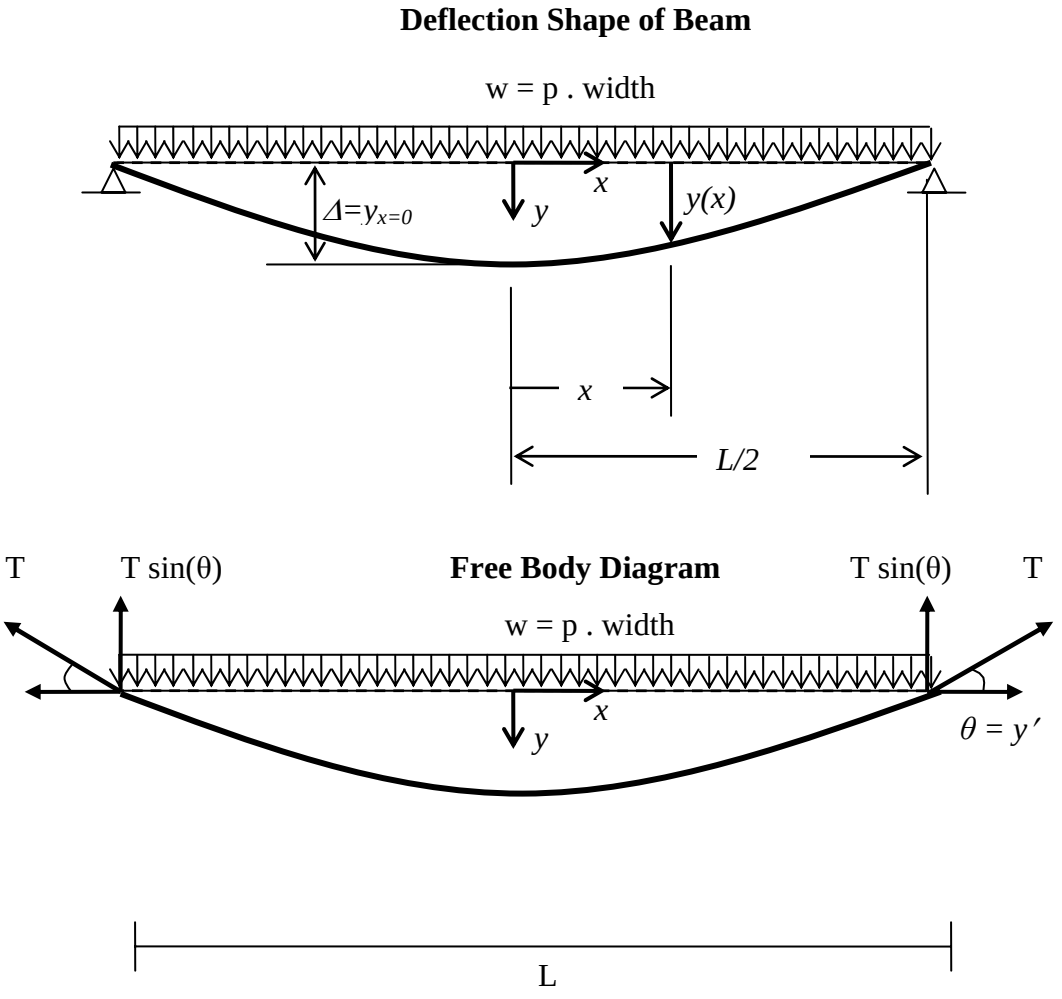

Figure 3.1 – Free Body Diagram and Deflected Shape of Sample

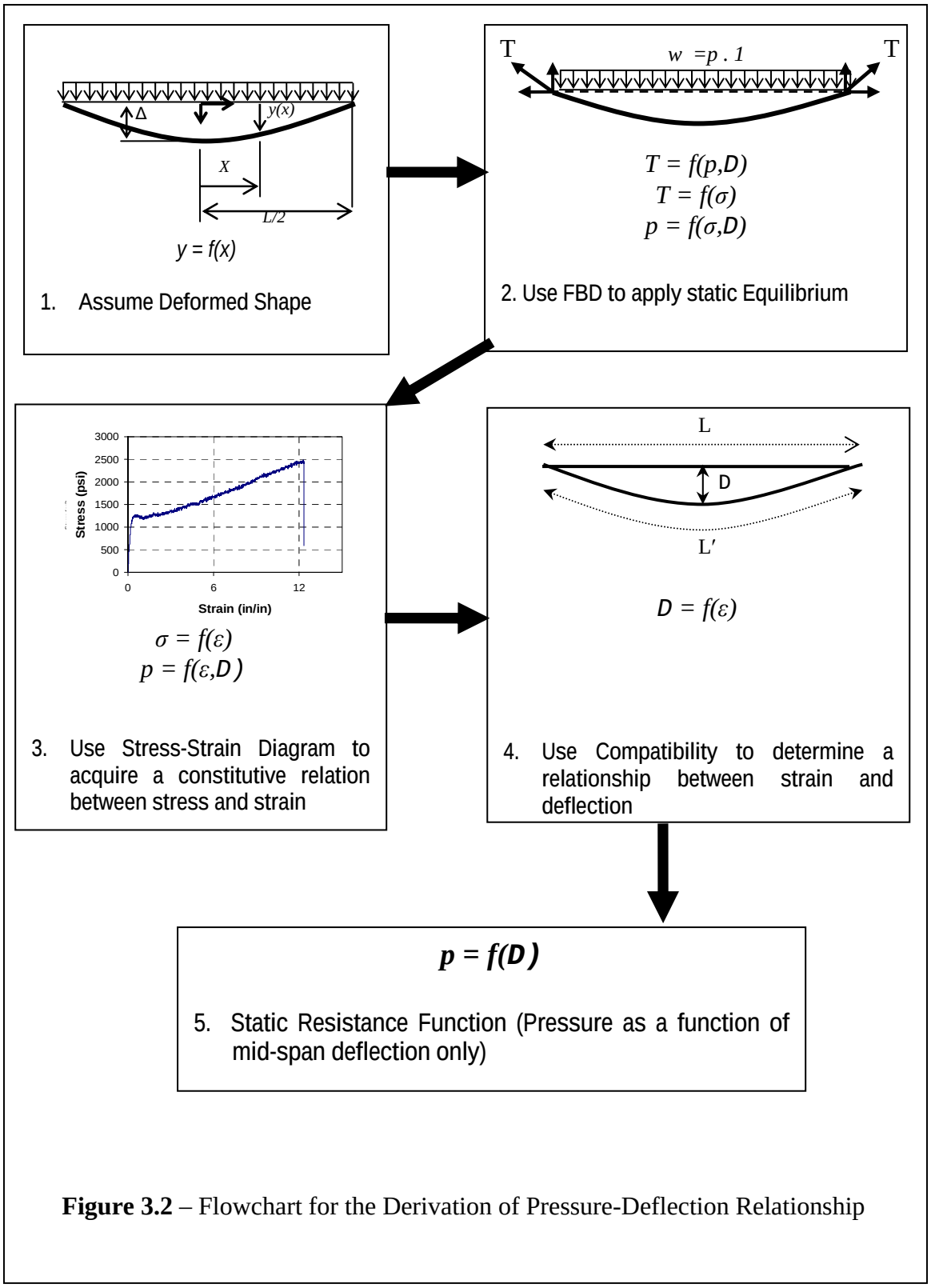

Figure 3.2 – Flowchart for the Derivation of Pressure-Deflection Relationship

Since the assumed shape is parabolic, the derivation begins with the general expression for a parabolic function to represent deflection as a function of x:

$$y=ax^2+bx+c \qquad (3.1)$$

Using known boundary conditions, constants a, b, and c are determined. First, b is determined; to do this, the derivative of Equation (3.1) is found.

$$y' = 2ax + b = 0,$$

The first boundary condition is

$$y' = 0 \text{ @ } x = 0,$$

which results in

$$b = 0.$$

Now Equation (3.1) reduces to,

$$y = ax^2+c$$

The second boundary condition is

$$y = \Delta \text{ @ } x = 0$$

Substituting gives,

$$y = \Delta = a(0)^2+c$$
$$or \qquad c = \Delta$$

The final boundary condition is,

$$y = 0 \text{ @ } x = \frac{L}{2}$$

Substituting gives,

$$y = a\left(\frac{L}{2}\right)^2 + \Delta = 0,$$

$$\text{or} \qquad a = -\frac{4\Delta}{L^2}.$$

Substituting constants a, b, and c back into Equation (3.1) gives the expression for *y* and *y'* as shown below:

$$y(x) = \Delta\left(1 - 4\left(\frac{x}{L}\right)^2\right) \tag{3.2}$$

$$y'(x) = -8\Delta\left(\frac{x}{L^2}\right) \tag{3.3}$$

Now that the parabolic shape is found, the next step is to use equilibrium to find a relationship between load and stress. From earlier research (Kennedy, 2005 and Dinan, 2005) it was found that the tension membrane force, T, varies along the length of the member with the smallest values at the mid point and the largest at the supports, which can vary up to approximately 10%. For simplicity, the tension force, T, is assumed to be constant, and the end values are used (Kennedy, 2005).

In Figure 3.1 the free body diagram of the polymer sheets can be seen. From equilibrium it is known that,

$$\Sigma F_y = 0$$
$$or \qquad 2\,T\sin(\theta) = wL \tag{3.4}$$

and for small angles, $\sin(\theta)$ can be approximated as θ, which is also equal to *y'* from Equation (3.3). Additionally, T can be rewritten a σA. Substituting this into Equation (3.4) yields,

$$2(\sigma A)\left(\frac{-8\Delta}{L^2}x\right) = wL$$

Substituting $x = \frac{L}{2}$,

$$2(\sigma A)\left(\frac{-8\Delta}{L^2}\frac{L}{2}\right) = wL$$

which simplifies and reduces to

$$\left(\frac{-8\sigma A}{L^2}\right)\Delta = w$$

Now using a unit width, *b=1*, the area, *A*, would be equal to *bt = (1)t = t*, and the distributed load, *w*, would then be *w = pb = p*, where *p* is the pressure. Substituting these parameters into the above equation yields,

$$p = \frac{-8\sigma \quad t}{L^2}\Delta \qquad (3.5)$$

Next, a relationship between Δ and σ is found through the constitutive relation of the material (stress-strain diagram).

The next step is to use compatibility to determine the relationship between strain and deflection. Once an exact strain is found, the corresponding stress can be determined from a stress-strain diagram. This produces pressure as a function of deflection (Static resistance function). This process is outlined next.

The first step of this process is to assume that strain is uniform along the length of the beam. It is known from the definition of strain that

$$L' = (1+\varepsilon)(L) \qquad (3.6)$$

Additionally, the arc length is given by

$$ArcLength = \int_0^L \sqrt{1 + (g'(x)^2)}$$

where $g'(x)$ may be replaced with y' from Equation (3.3).

Now, let $\beta = \frac{-8\Delta}{L^2}$. Then the arc length may be written as

$$ArcLength = 2\int_0^{\frac{L}{2}} \sqrt{1 + \beta^2 x^2}\ . \qquad (3.7)$$

Using integration tables,

$$\int \sqrt{x^2 + \alpha^2} = \frac{x\sqrt{x^2 + \alpha^2}}{2} + \frac{\alpha^2}{2} \ln\left(x + \sqrt{x^2 + \alpha^2}\right). \qquad (3.8)$$

Next, the equation is manipulated to make the right side of Equation (3.7) similar in form to the left side of Equation (3.8). Since L' is the arc length, the following relation applies:

$$L' = 2\int_0^{\frac{L}{2}} \sqrt{1 + \beta^2 x^2}\, dx$$

$$= 2\int_0^{\frac{L}{2}} \beta \sqrt{\left(\frac{1}{\beta^2} + x^2\right)} dx\ .$$

$$= 2\beta\int_0^{\frac{L}{2}} \sqrt{\alpha^2 + x^2}\, dx$$

where $\alpha = \frac{1}{\beta}$.

So, from substituting the above relationship for L' into Equation (3.8), it is seen that

$$L' = 2\beta\left[\frac{x\sqrt{x^2 + \alpha^2}}{2} + \frac{\alpha^2}{2} \ln\left(x + \sqrt{x^2 + \alpha^2}\right)\right]_0^{\frac{L}{2}}.$$

Solving the integral using the integration limits and back-substituting the values for α and β, it is finally shown that

$$L' = 2\left(\frac{-8\Delta}{L^2}\right)\left[\frac{\frac{L}{2}\sqrt{\frac{L^2}{4}+\frac{L^4}{64\Delta^2}}}{2} + \frac{L^4}{128\Delta^2}\ln\left(\frac{L}{2}+\sqrt{\frac{L^2}{4}+\frac{L^4}{64\Delta^2}}\right) - \left(\frac{L^4}{128\Delta^2}\ln\left(\frac{L^2}{8\Delta}\right)\right)\right]. \qquad (3.9)$$

The following summarizes the remaining steps to determine the detailed analytical model:

1. Set Δ equal to zero and incrementally increase the value by a small amount
2. Use Equation (3.9) to determine the corresponding value for L'
3. Use Equation (3.6) to calculate the strain
4. From the stress-strain curve, find the stress corresponding to the calculated strain
5. Use Equation (3.5) to calculate the pressure
6. Increment Δ and start at step #2 again. Repeat process until the ductility limit is reached or failure in the polymer is predicted.
7. Plot the calculated pressures versus the incremented deflections

The analytical procedure described above was used to develop the resistance function of the polymer shown in Figure 3.3a. The true stress-strain relationship was used to develop the resistance for a 1/8-in. thick polymer sheet on a 12-ft. high wall as shown in Figure 3.3b. Although Figure 3.3b indicates that the polymer could deflect up to 60 in. and provide a resistance of 4 psi before failure, other factors could produce failure and not allow the polymer to utilize its full ductility. Failures due to stress concentrations at the connections and/or localized over stressed regions at mortar joints

could control the resistance. Preliminary research (Beckman, 2005 and Bechtold, 2004) has indicated that these effects are critical, and additional research is needed to evaluate all failure limit states, other than the ductility limit state, which could control the ultimate resistance of a blast retrofitted concrete wall using polymers.

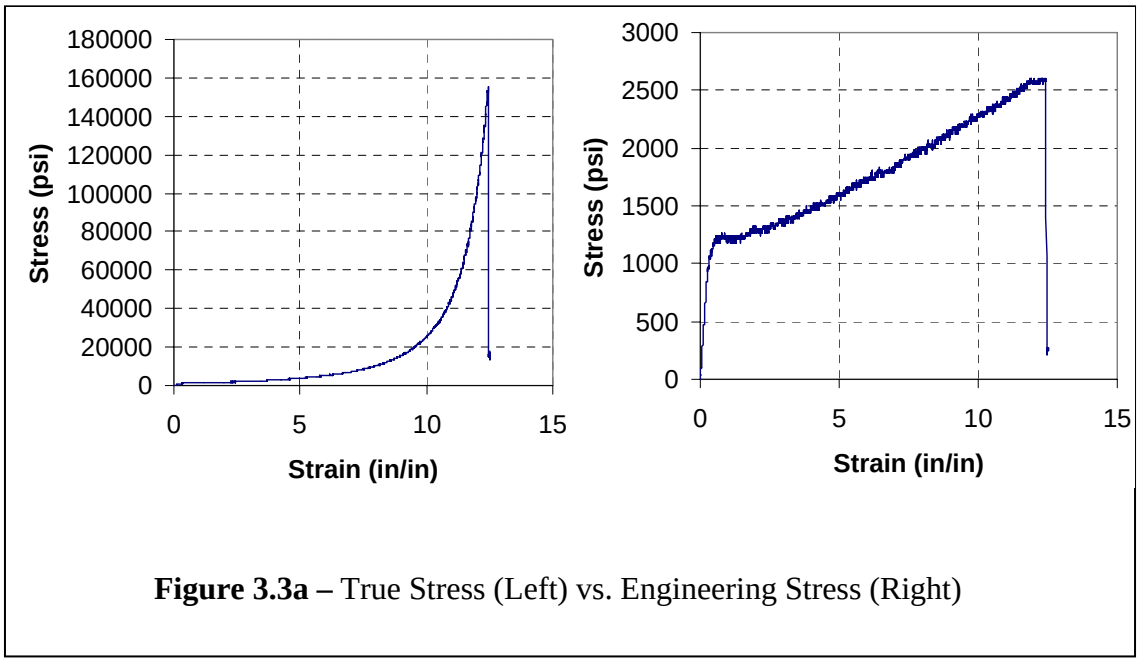

Figure 3.3a – True Stress (Left) vs. Engineering Stress (Right)

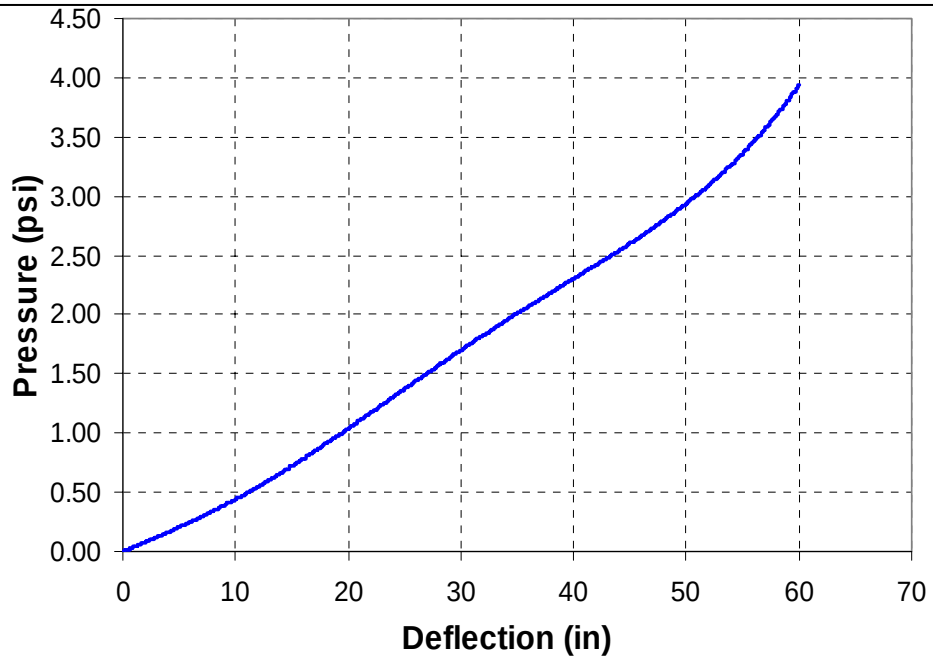

Figure 3.3b - Static Resistance Function of Polymer from Figure 3.3a

CHAPTER 4 – EXPERIMENTAL EVALUATION

4.1 General

Once the analytical model for the static resistance function was formulated, it was necessary to verify the model experimentally. To do this, three levels of experimental evaluations were performed. Each test helped to verify the predicted analytical model.

4.2 Coupon Testing

4.2.1 Setup and Procedure

The first set of tests was coupon testing. Coupons cut from the polymer sheets were tested under uniaxial tension to failure using a 2 inch per minute head speed. The coupons were tested following the ASTM D638 standard shown in Figure 4.1.

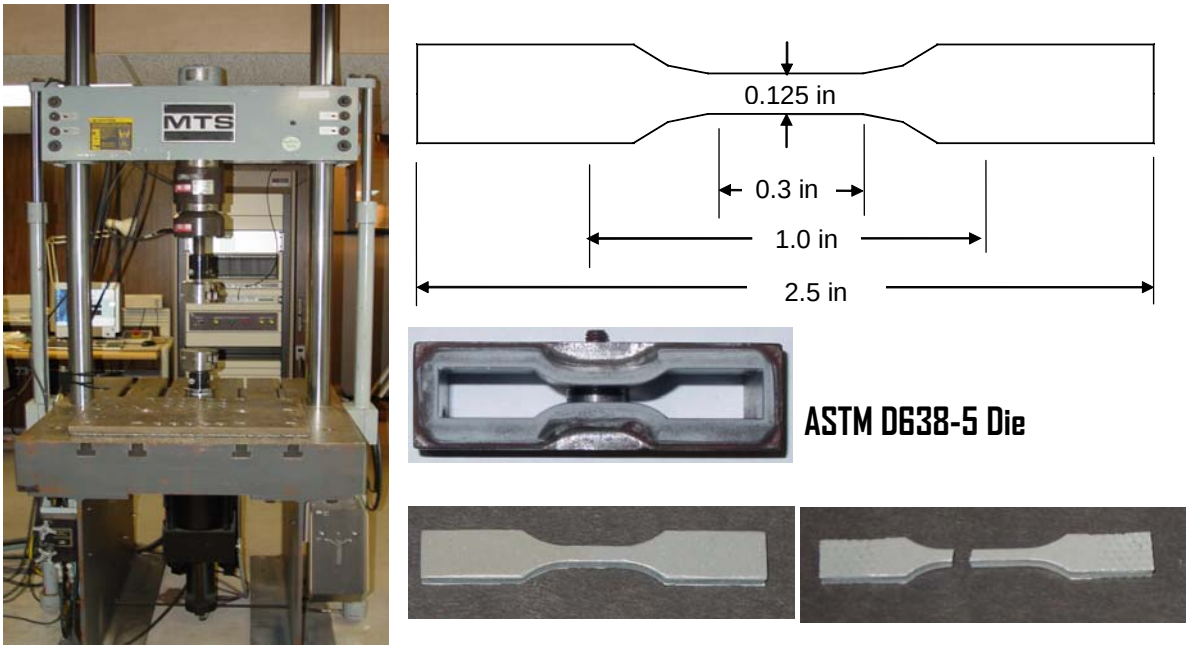

Figure 4.1 – Coupon Testing Setup

For this part of the study, there were a total of 12 coupons tested at AFRL. Six of the coupons were cut longitudinally and six were cut transversely from the polymer sheet. This was done to ensure that the polymer is isotropic at all locations. Additionally, because the polymer's thickness varied, many coupons were needed to get an overall average for the sheet. Once the data was collected, the maximum tensile stress, elongation at the maximum tensile stress, the maximum elongation percentage, secant modulus, and toughness were calculated for the samples.

4.2.2 Calculating True Stress from Engineering Stress

The stress-strain diagrams produced throughout the testing depicts engineering stress and corresponding strain. Since the polymer may undergo large deformations resulting in significant reduction of the original thickness of the samples during a blast, it is necessary to use the true stress-strain relation instead of the engineering property. The difference between engineering stress and true stress is that engineering stress assumes there is no or very little reduction in area as the specimen is loaded. This assumption works well for most civil engineering structures because the structures are only allowed to deflect a very small amount. However, under blast loading, there is a large amount of deflection, and this assumption doesn't work well. For modeling the polymer sheets, true stress was used. Figure 4.2 shows a comparison between true and engineering stress for the LS V1a sample. From the figure, it can be seen that as the load is increased, the true stress begins to differ greatly from engineering stress. Similar calculations were done for each coupon.

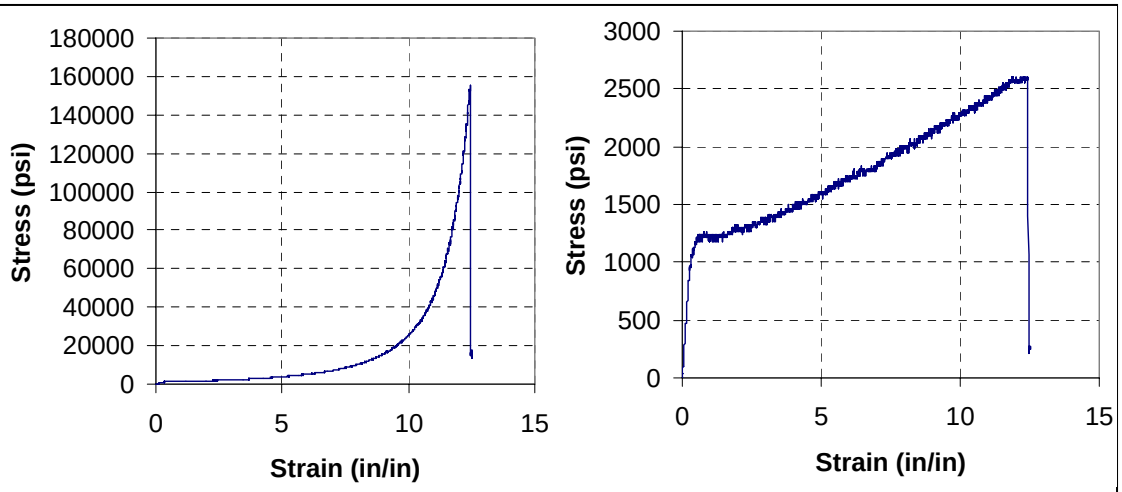

Figure 4.2 – True Stress (Left) vs. Engineering Stress (Right) for LS V1a Sample

4.2.3 Results

Figure 4.3 shows the engineering stress versus strain for all 12 coupons. Also, the maximum tensile stress, elongation at the maximum tensile stress, the maximum elongation percentage, secant modulus, and toughness for each coupon are shown in Table 4.1.

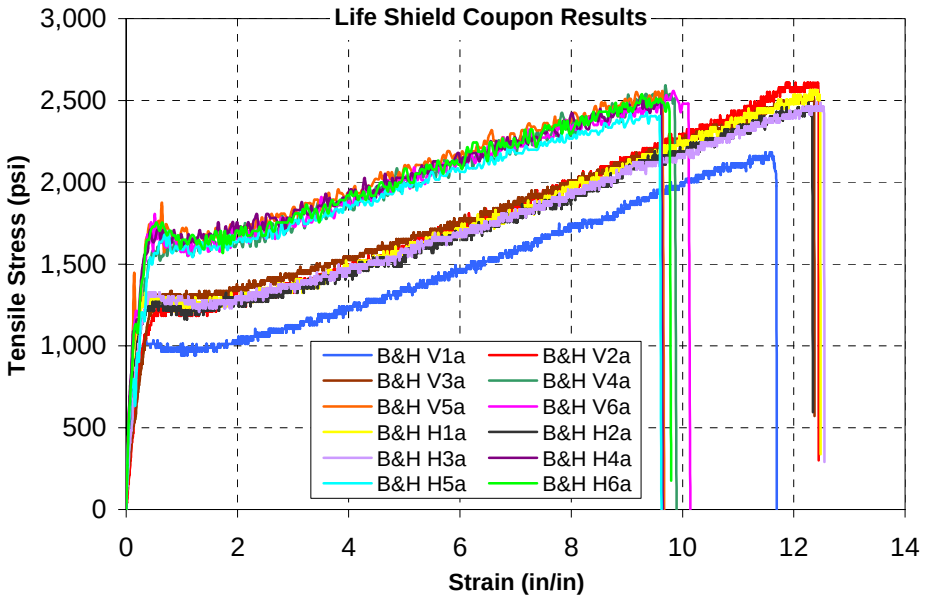

Figure 4.3 - Stress-strain Results of Tensile Tests on Coupon Samples

Table 4.1 - Coupon Test Results for Sheet Polymer Samples

Sample Name	Maximum Tensile Strength psi	Elongation at Max. Tensile Strength %	Maximum Elongation %	Secant Modulus psi	Toughness psi*in/in
LS H1a	2,563	1229.05	1247.89	273	22,057
LS H2a	2,485	1226.29	1234.11	293	21,272
LS H3a	2,486	1241.23	1255.19	0	21,900
Mean	2,511	1232.19	1245.73	189	21,743
LS H4a	2,523	924.95	964.82	4,484	19,224
LS H5a	0	-0.17	962.18	3,464	18,449
LS H6a	2,538	926.61	979.76	4,451	19,545
Mean	1,687	617.13	968.92	4,133	19,073
LS V1a	2,183	1149.30	1169.30	234	17,190
LS V2a	2,608	1186.07	1244.96	280	22,110
LS V3a	2,542	1230.03	1237.27	327	22,163
Mean	2,444	1188.47	1217.18	280	20,488
LS V4a	2,593	969.47	989.35	3,392	19,545
LS V5a	2,551	917.08	967.18	4,243	19,544
LS V6a	2,557	983.72	1013.94	3,930	20,197
Mean	2,567	956.76	990.16	3,855	19,762
Overall Mean	**2,302**	**999**	**1,105**	**2,114**	**20,266**

4.2.4 Summary and Conclusions

Coupon testing was an important step in the determination of the constitutive relationship of the polymer sheets. It was very important to obtain ductility limits and maximum applied stresses to continue the development of the static resistance function. Additionally, values obtained from the stress-strain diagrams were used in the dynamic modeling portion of the research. Next, the connection-level testing of the polymer is presented.

4.3 Connection Testing

4.3.1 General

Polymers are capable of absorbing a great deal of energy which could make them a useful retrofit for CMU walls. One problem with using polymers is developing an effective connection method to allow them to utilize their full potential of high ductility. The most economical and installation-friendly way to connect the polymer is to bend the polymer and use a steel connection plate to bolt it to the floor and ceiling. This increases the absorption capability of the CMU wall and reduces or eliminates fragments of the wall coming into the interior space. In order for the polymer to reach its full capacity, well-designed connections must be used to prevent premature failure at the floor and ceiling. To find the most effective and practical connection method, 15 connection tests were performed using various bolt spacing and connection plate thicknesses. The bolt spacings used were 8, 12, and 16 in., and the connection plate thicknesses used were 0.125 in. and 0.25 in.

4.3.2 Setup and Procedure

In this section, a detailed description of the setup and procedure to achieve the most efficient connection method is provided.

The polymer samples were bent at a 90-degree angle and bolted between a rigid channel and a steel connection plate. The length of the bend between the channel and the plate was 6 in., and the bolts were centered on the plate 3 in. from each side. The top channel was connected to an MTS machine that loaded the polymer sample in tension. This setup is illustrated in Figure 4.4.

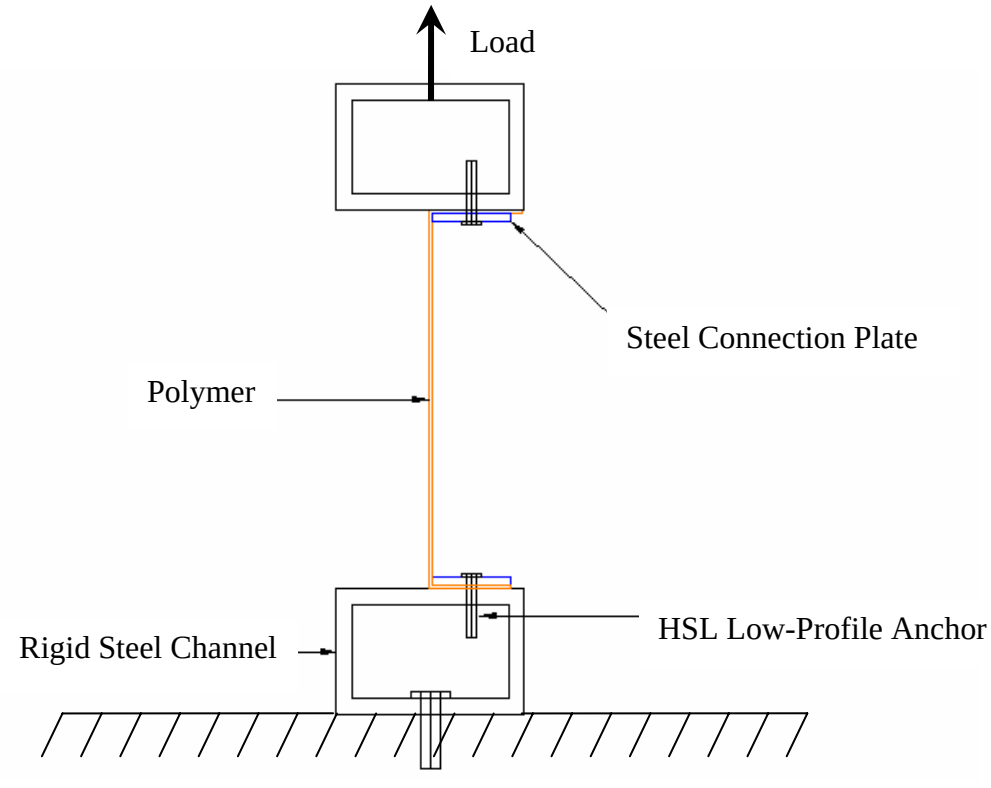

Figure 4.4– AutoCAD Depiction of the Connection Test Setup

The polymer was tested using two thicknesses, which were 0.125 in. and 0.16 in. Additionally, the bolt spacing and the steel connection plate thickness varied. There were

three different bolt spacings of 8, 12, and 16 in., and two connection plate thicknesses of 0.125 and 0.25 in. After several tests were completed, it was decided that the length of the samples should be reduced from 24 in. to 6 in. in order to fail the samples since the travel on the MTS machine is limited. The width remained a constant 36 in. and each bolt was torqued to 1600 lb-in.

With regard to applied torque on the bolts, Hilti Anchors are commonly used in the field, and the HSL low-profile heavy-duty sleeve anchors apply a uniform torque of 1600 lb-in. to each bolt. The bolts used to attach the polymer were 5/8-in. high-strength bolts. A picture of the actual setup can be seen in Figure 4.5. Failure was sudden and could have initiated at either of the edges where the steel plate might have "cut" into the polymer sample.

Figure 4.5 - Picture of the Connection Setup

Once the polymer was in place, the MTS machine loaded the sample. Due to the high deflection limits of the polymer, the MTS machine ran out of travel before failing any of the samples. Despite this, sufficient data was collected, and optimal spacing and connection plate thicknesses were obtained. Recently, a very short sample was tested to failure to ensure that no significant response characteristics were missed in the samples that did not fail. The sample tested showed no significant response characteristics before failure. The polymer tore in a jagged manner mainly in the gage length. Figure 4.6 shows the polymer after the test. Failure was sudden and could have initiated at either of the edges where the steel plate might have "cut" into the polymer sample.

Figure 4.6 – Failure of Polymer Sample

4.3.3 Results

In order to test all parameters to develop the most optimal design, a connection test matrix was developed for the connection experiments. Table 4.2 shows the results of the 16 tests performed to develop the most effective connection. Figures 4.7-4.36 show the test setup of all 17 samples and their response during various stages of the tests. These figures also show the load-displacement response of all samples.

Table 4.2 – Results from Connection Testing

Sample #	Test sample name	Sample length, *L* (in)	Sample thickness, *t* (in)	Clamping plate thickness, t_P (in)	Anchor spacing, *s* (in)	Energy absorbed (lb-in)
1	LS-C1b	18	0.125	0.125	12	24,780
2	LS-C2	36	0.125	0.25	12	19,893
3	LS-C2b	18	0.125	0.25	12	27,296
4	LS-C3	36	0.125	0.125	8	13,506
5**	LS-C3**	36	0.125	0.125	8	17,428
6	LS-C3b	18	0.125	0.125	8	25,593
7	LS-C4b	18	0.125	0.25	8	27,847
8	LS-C5	36	0.160	0.125	12	23,143
9	LS-C5b	18	0.160	0.125	12	30,804
10	LS-C6	36	0.160	0.25	12	27,641
11	LS-C6b	18	0.160	0.25	12	32,840
12	LS-C7b	18	0.160	0.125	8	17,717
13	LS-C8	36	0.160	0.25	8	20,212
14	LS-C8b	18	0.160	0.25	8	43,541
15	LS-C9	18	0.125	0.125	16	24,461
16	LS-C10	18	0.160	0.125	16	34,632

** Test repeated twice

Figure 4.7 - Test Sample LS-C1b

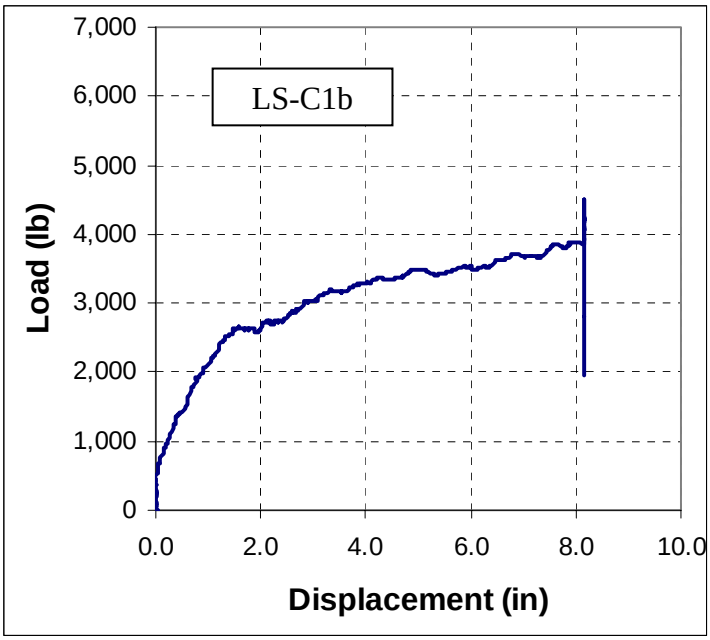

Figure 4.8 - Load-deflection Curve for LS-C1b

Figure 4.9 - Test Sample LS-C2

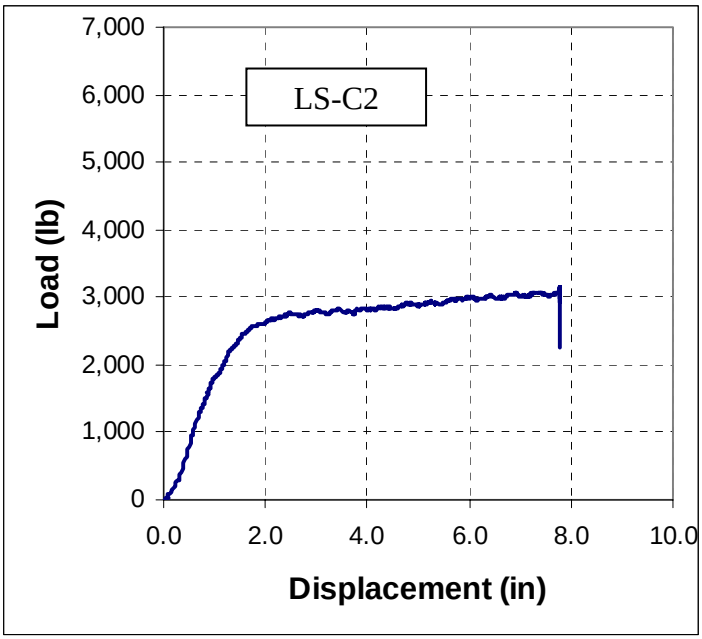

Figure 4.10 - Load-deflection Curve for LS-C2

Figure 4.11 - Test Sample LS-C2b

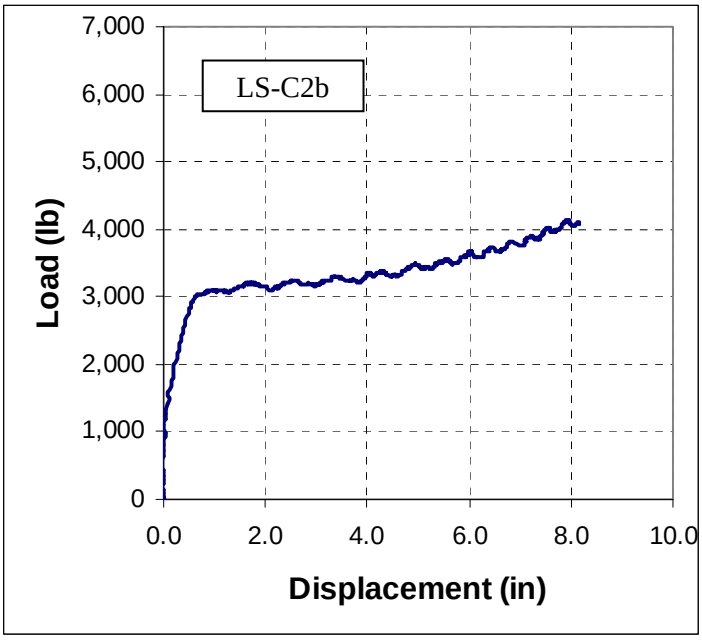

Figure 4.12 - Load-deflection Curve for LS-C2b

Figure 4.13 - Test Sample LS-C3

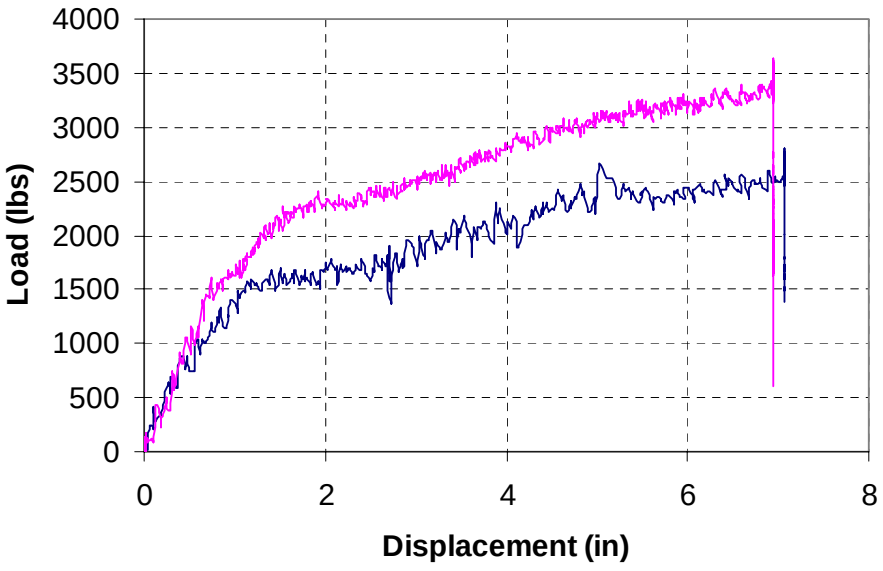

Figure 4.14 - Load-deflection Curve for LS-C3 (Both Tests)

Figure 4.15 - Test Sample LS-C3b

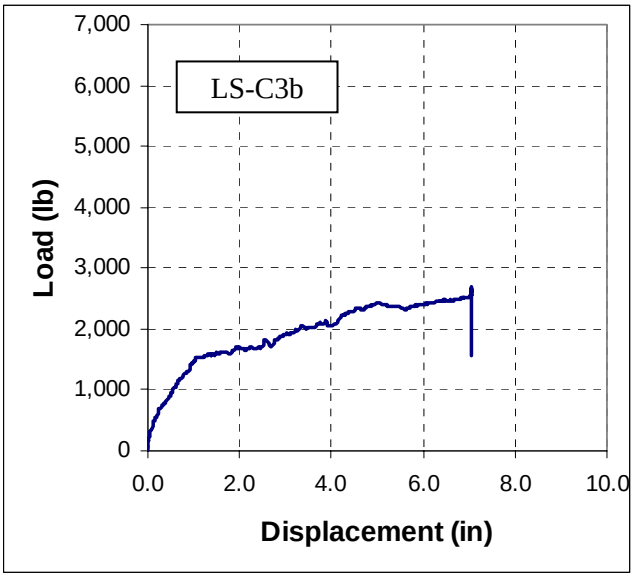

Figure 4.16 - Load-deflection Curve for LS-C3b

Figure 4.17 - Test Sample LS-C4b

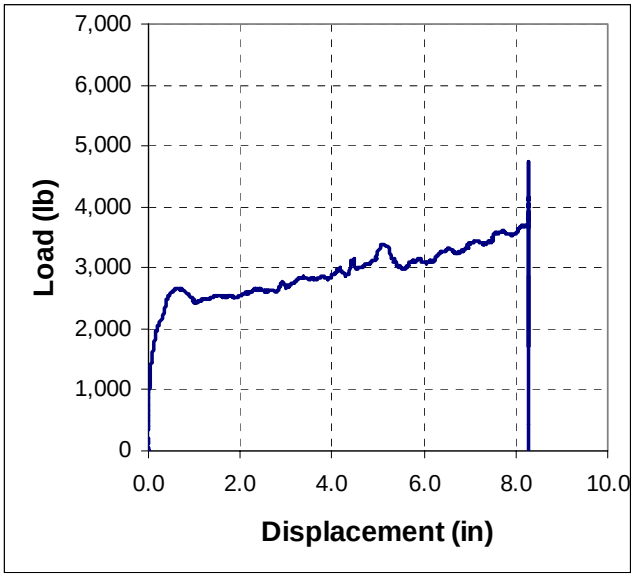

Figure 4.18 - Load-deflection Curve for LS-C4b

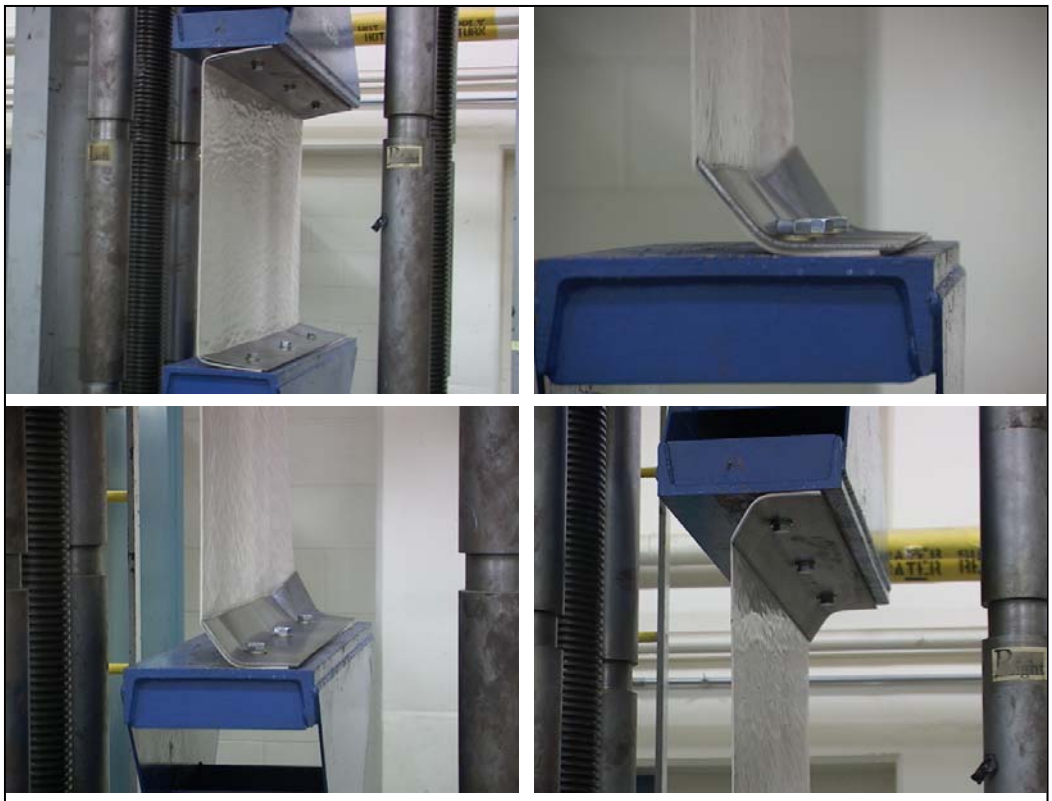

Figure 4.19 - Test Sample LS-C5

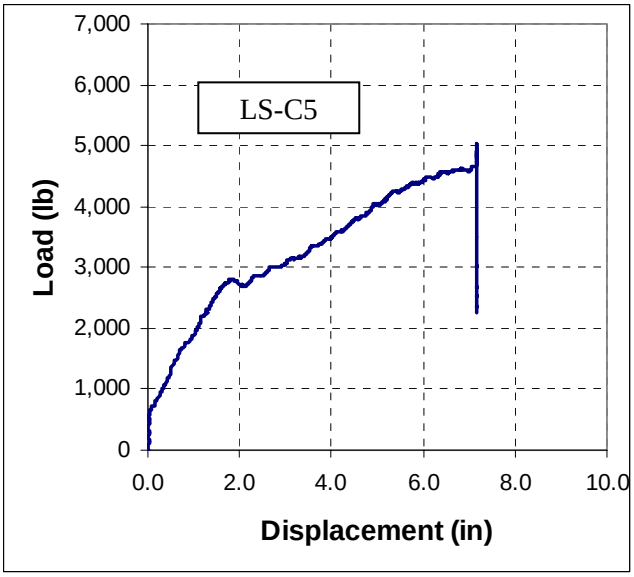

Figure 4.20 - Load-deflection Curve for LS-C5

Figure 4.21 - Test Sample LS-C5b

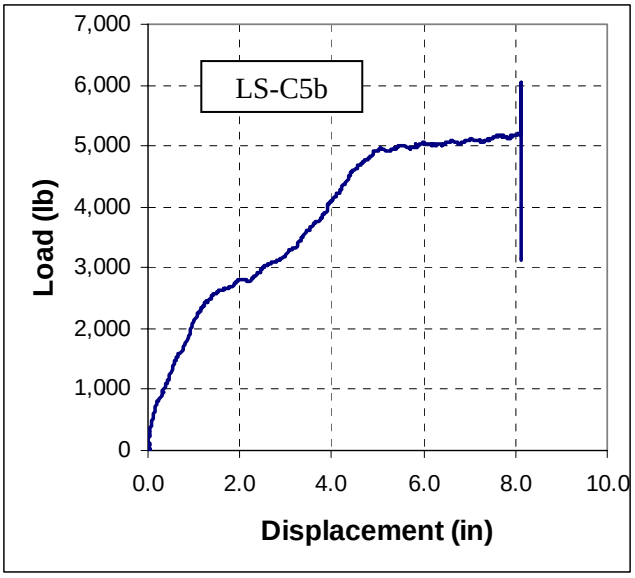

Figure 4.22 - Load-deflection Curve for LS-C5b

Figure 4.23 - Test Sample LS-C6

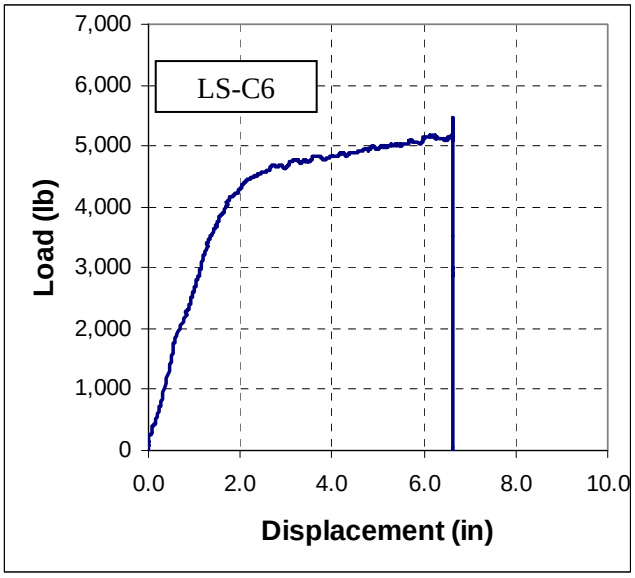

Figure 4.24 - Load-deflection Curve for LS-C6

Figure 4.25 - Test Sample LS-C6b

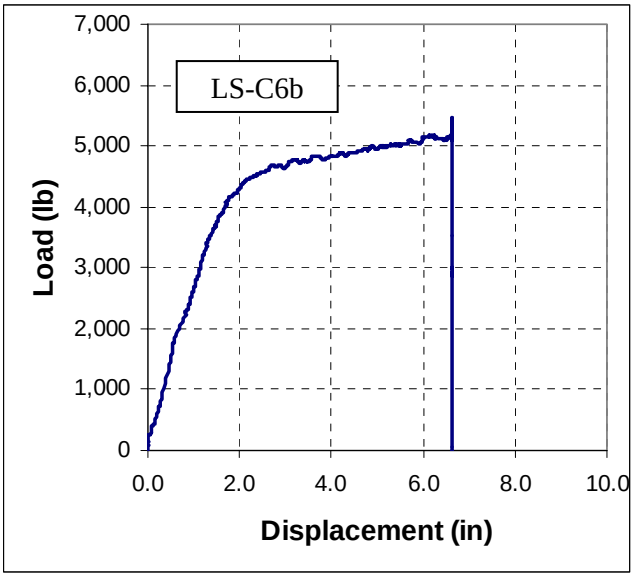

Figure 4.26 - Load-deflection Curve for LS-C6b

Figure 4.27 - Test Sample LS-C7b

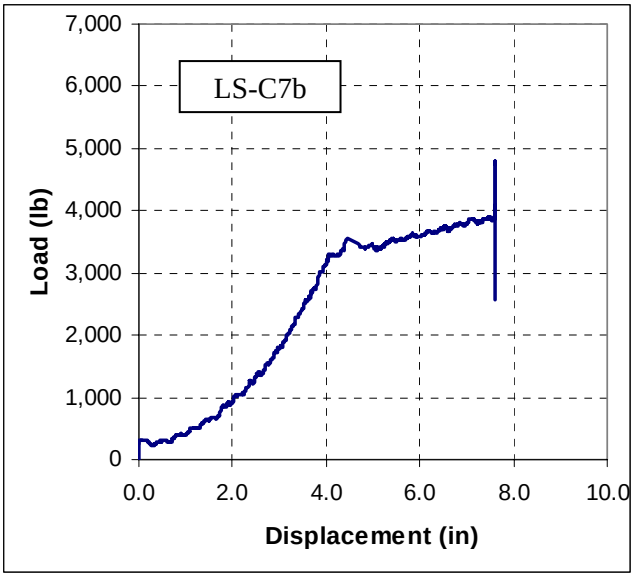

Figure 4.28 - Load-deflection Curve for LS-C7b

Figure 4.29 - Test Sample LS-C8

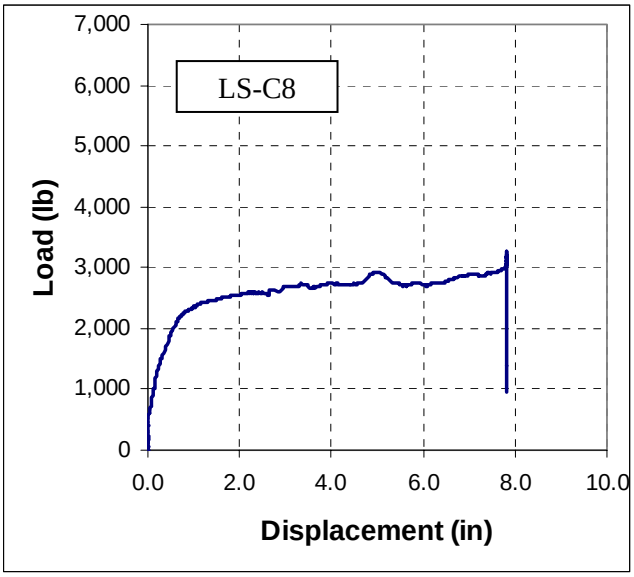

Figure 4.30 - Load-deflection Curve for LS-C8

Figure 4.31 - Test Sample LS-C8b

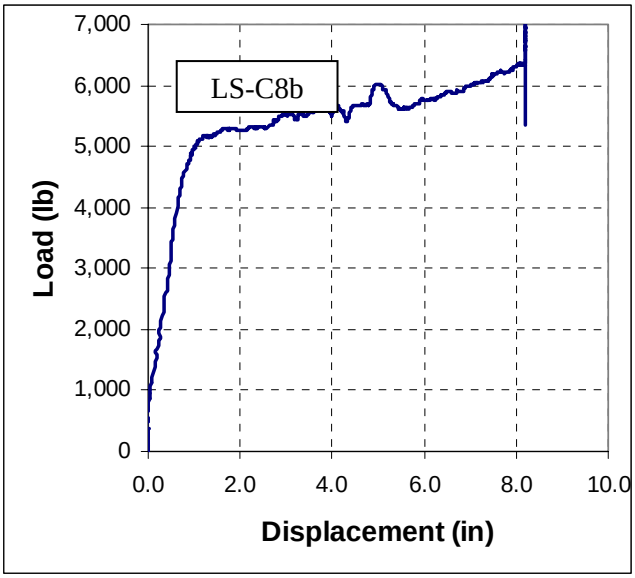

Figure 4.32 - Load-deflection Curve for LS-C8b

Figure 4.33 - Test Sample LS-C9

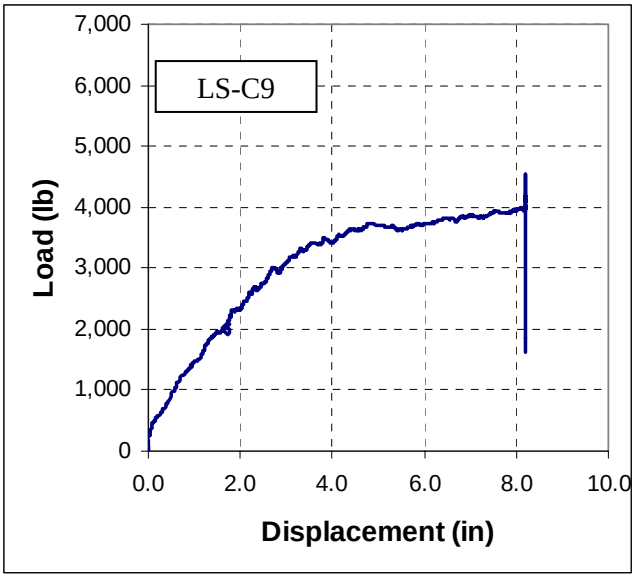

Figure 4.34 - Load-deflection Curve for LS-C9

Figure 4.35 - Test Sample LS-C10

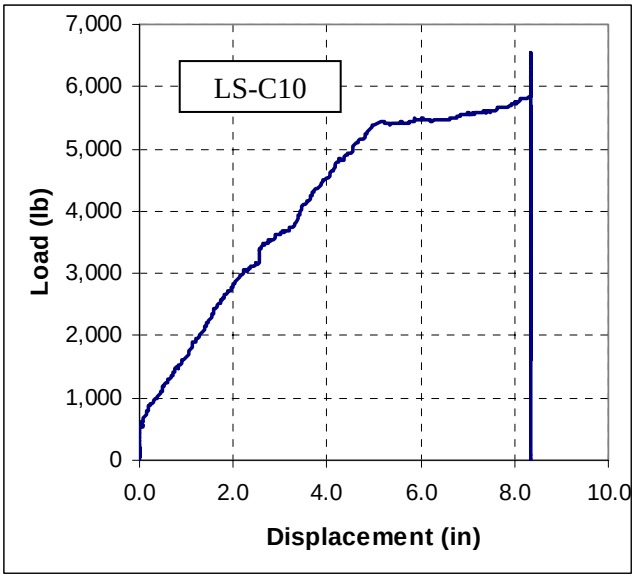

Figure 4.36 - Load-deflection Curve for LS-C10

4.3.4 Summary and Conclusions

After analyzing the data, it can be seen that by choosing certain parameters, the polymer sheet is allowed to develop most of its full capacity. One of the main reasons for running connection tests was to find what connection plate thickness should be used in order for the polymer to not tear out at the bolts causing premature failure. From observations during the tests and from the pictures, it was shown that a 1/4-in. connection plate should be used to provide enough clamping resistance to prevent tear out at the connection. From observations during the tests using the 1/8-in. connection plate thickness, it was shown that the plate deformed upward. In some retrofitted systems, bending of the plate can add ductility which in turn would cause greater energy absorption capability of the system. However, for this retrofit system, there is plenty of ductility provided by the polymer. Besides, this would cause the polymer to tear out from the bolt holes in the polymer sheet which would cause premature failure.

The next parameter that was varied during the tests was the bolt spacing. There were three spacings chosen for the test which were 8 in., 12 in., and 16 in. The idea was to see how far the bolts could be spaced without losing energy absorption or allowing the connection plate to bend causing the polymer to tear out at the connection. It was found that 16 in. was the optimal spacing for the bolts. It was also shown that 12 in. worked well too, so it was decided that both spacings should be used in the component testing (Section 4.3).

The final parameter that was varied was the thickness of the polymer. The polymer had two thicknesses, 0.125 in. and 0.160 in. For most of the tests, the energy

absorption was much greater using the 0.160 in. sample thickness. For the component beam tests, both the 0.125 in. and 0.160 in. thicknesses were evaluated.

These tests showed that by finding the right combination of parameters, the energy absorption capabilities of the polymer sheets can be greatly increased. This is because the polymer sheets are allowed to reach their full capacity. It is the recommendation of this research that a 1/4-in. connection plate and 16 in. bolt spacing be used for optimum energy absorption.

One note should be made about an observation on how the connection plate edges could reduce the strength of the polymer if there are sharp edges present. In these tests, the polymer sheets were not extended beyond the plate end, preventing the corner of the plate from tearing into the polymer. It is expected that a sharp corner could significantly reduce the polymer tear strength. Such results of this premature failure were observed in the steel sheet retrofit system (Kennedy, 2005). The sharp edges reduced the tensile capacity of the steel sheets by more that 50%. As a result, this should be avoided to prevent premature tearing of polymer sheets.

Additionally, a table was made to compare the maximum theoretical load to the experimental load obtained from the connection tests (Table 4.3). From the table, several observations can be made. All of the samples with shorter gage length utilized more of their theoretical capacity compared to the samples with identical parameters except gage length. This is because the shorter samples were loaded closer to failure than the longer samples. The sample that produced the highest percent capacity was LS-C8b. This sample had a gage length of 6 in., a thickness of 0.160 in., used a connection plate thickness of 0.25 in., and anchor spacing of 8 in.

Table 4.3 - Theoretical Capacity Compared with Experimental Capacity

Sample Name	Theoretical Capacity	Experimental Capacity	
	P_{max} (kip)	P_{max} (kip)	% of Capacity
LS-C1b	10.35	3.88	37.49
LS-C2	10.35	3.05	29.47
LS-C2b	10.35	4.1	39.61
LS-C3	10.35	2.45	23.67
LS-C3**	10.35	3.32	32.08
LS-C4b	10.35	3.72	35.94
LS-C5	13.248	4.61	34.80
LS-C5b	13.248	5.17	39.02
LS-C6	13.248	5.04	38.04
LS-C6b	13.248	5.24	39.55
LS-C7b	13.248	3.87	29.21
LS-C8	13.248	2.98	22.49
LS-C8b	13.248	6.35	47.93
LS-C9	10.35	3.94	38.07
LS-C10	13.248	5.73	43.25

4.4 Component Beam Testing

4.4.1 General

The final level of testing was the component beam test. The component beams were subjected to a uniform static load and used the optimal connections obtained from the connection tests. Once tested, the results were compared to the analytical model predicted in Chapter 3.

4.4.2 Setup and Procedure

The component beam tests used polymer sheets cut 11 ft. long and 22 in. wide. With the 6 in. that was bent on each side, the gage length of the sample became 10 ft. There were two thicknesses tested which were 0.125 in. and 0.16 in. For all tests, a ¼-in. connection plate was used. Two bolt spacings of 12 and 16 in. were tested. The test matrix is shown in Table 4.4. The samples were tested using a 16-point loading tree closely simulating a uniform load on the sheets. An AutoCAD drawling of the 16-point

loading tree is shown in Figure 4.37a. Figure 4.37b shows a polymer sample in the 16-point loading tree at the beginning of the test. Figure 4.37c shows the polymer nearing the end of the test. The mechanical connection at the beginning and during the test is shown in Figure 4.37d.

Table 4.4 - Component Beam Test Matrix

Test #	Sample Name	Sample thickness, t (in)	Connection plate thickness, t_P (in)	Hole Spacing, s (in)	Sample Size (in)
1	LS-T1	0.125	0.25	12	22x120
2	LS-T2	0.125	0.25	16	22x120
3	LS-T3	0.160	0.25	12	22x120
4	LS-T4	0.160	0.25	16	22x120

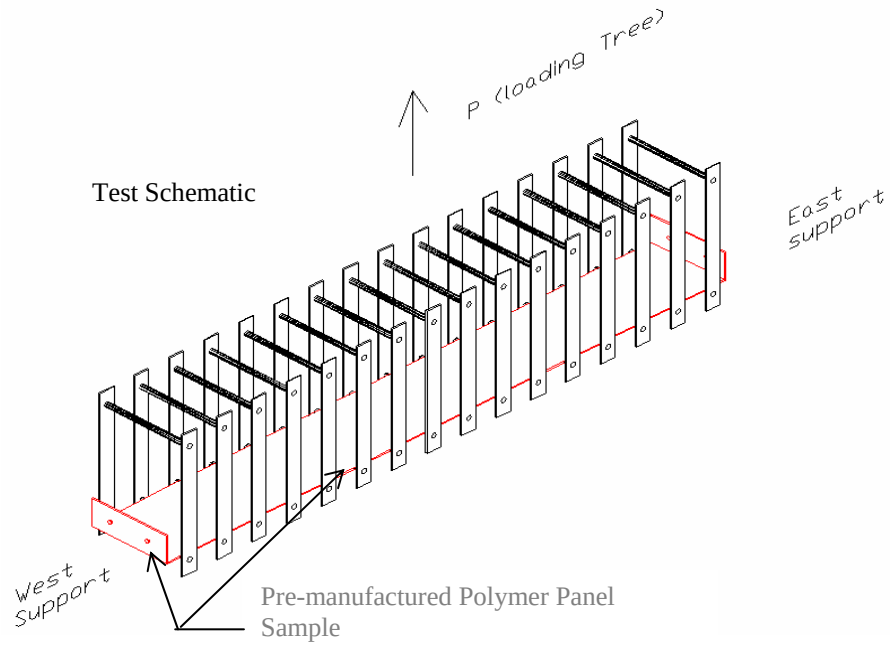

Figure 4.37a - AutoCAD Drawing of the 16-point Loading Tree

Figure 4.37b - Polymer Sample at the Beginning of the Test

Figure 4.37c - Polymer Sample Nearing the End of the Test

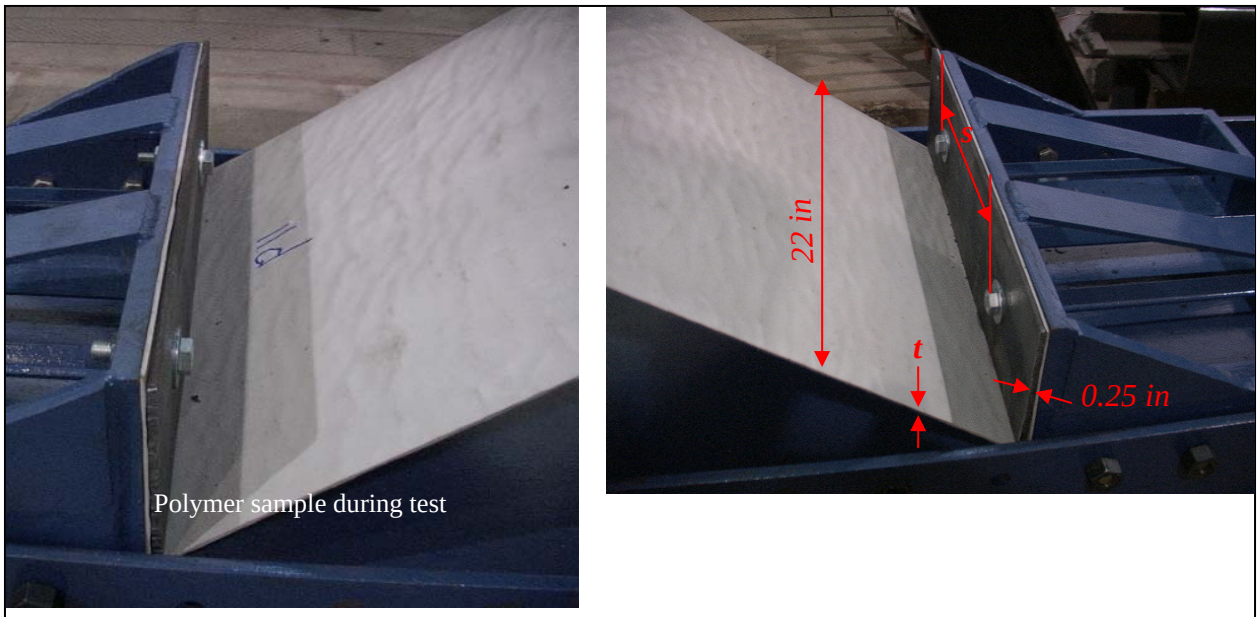

Figure 4.37d - Connection at the Beginning (Left) and During the Test (Right)

During the tests, the load-deflection data were recorded using a loading cell and three spring potentiometers. The potentiometers were placed at quarter points along the sample (Figure 4.38). The potentiometers and loading cell were connected to LabView, where load and deflection was recorded. Once the load and deflection was collected, they were used to calculate the equivalent pressure-displacement response (Static Resistance Function) of the blast mitigation system, which was then compared to the analytical model of the static resistance.

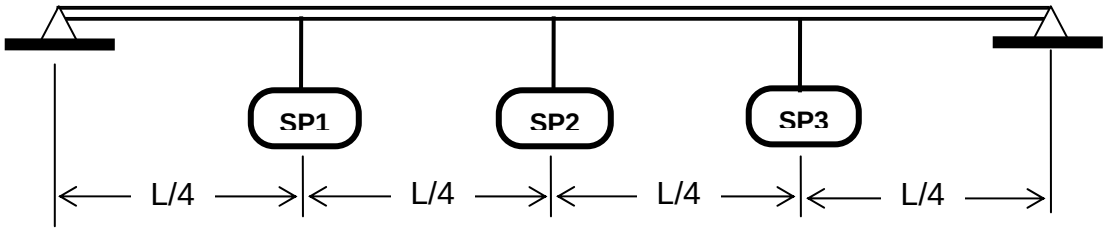

Figure 4.38 – Location of Displacement Devices for Component Beam Tests

4.4.3 Results

Component test LS-T1:

Sample LS-T1 had a thickness of 0.125 in. and used a 12 in. bolt spacing for the connections. Due to the loading cell having a maximum deflection of 20 in., the polymer sheet never reached failure. However, there was enough data to compare to the analytically predicted model. To predict the model, stress-strain relations attained from coupon testing were used. The comparison of the experimental data recorded from LS-T1 and the analytical model is shown in Figure 4.39.

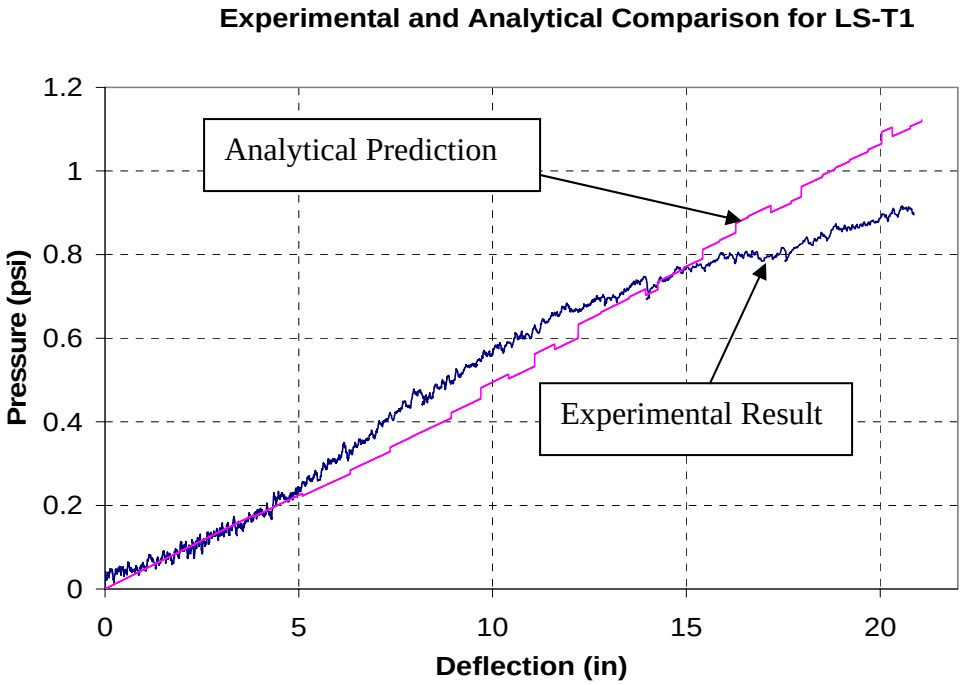

Figure 4.39 - Comparison of Experimental vs. Analytical Data for LS-T1

Component test LS-T2:

Sample LS-T2 had a thickness of 0.125 in. and used a 16 in. bolt spacing for the connections. Due to the loading cell having a maximum deflection of 20 in., the polymer sheet never reached failure. However, there was enough data to compare to the analytically predicted model. To predict the model, stress-strain relations attained from coupon testing were used. The comparison of the experimental data recorded from LS-T2 and the analytical model is shown in Figure 4.40.

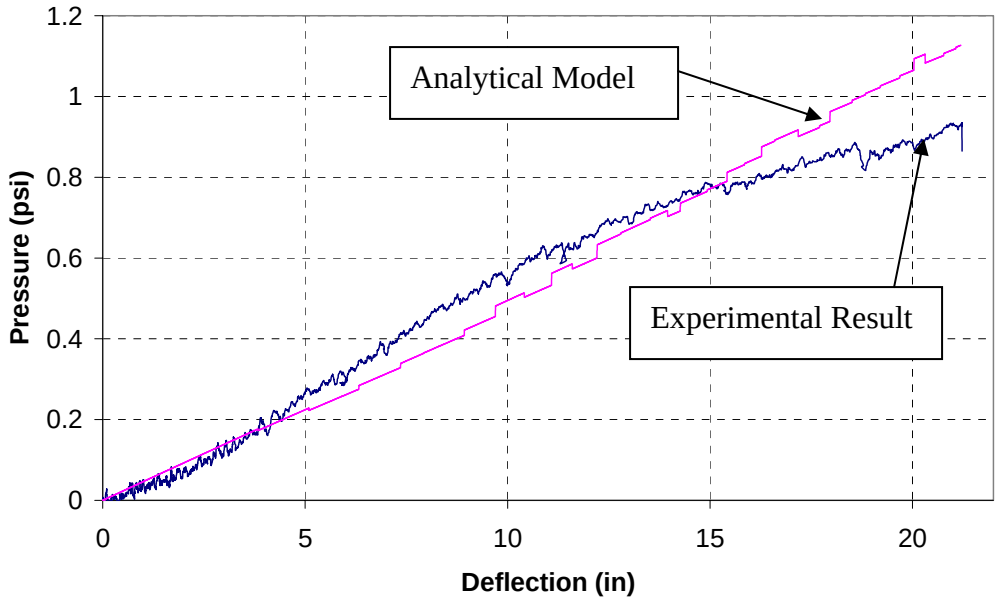

Figure 4.40 - Comparison of Experimental vs. Analytical Data for LS-T2

Component test LS-T3:

Sample LS-T3 had a thickness of 0.16 in. and used a 12 in. bolt spacing for the connections. Due to the loading cell having a maximum deflection of 20 in. the polymer sheet never reached failure. However, there was enough data to compare to the analytically predicted model. To predict the model, stress-strain relations attained from coupon testing were used. The comparison of the experimental data recorded from LS-T3 and the analytical model is shown in Figure 4.41.

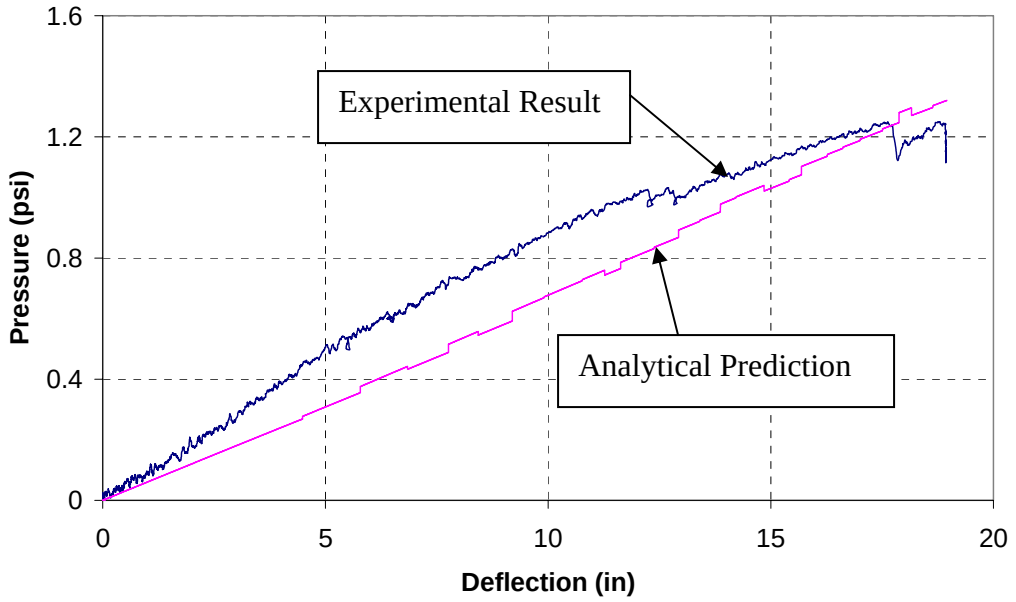

Figure 4.41 - Comparison of Experimental vs. Analytical Data for LS-T3

Component test LS-T4:

Sample LS-T4 had a thickness of 0.16 in. and used a 16 in. bolt spacing for the connections. Due to the loading cell having a maximum deflection of 20 in. the polymer sheet never reached failure. However, there was enough data to compare to the analytically predicted model. To predict the model, stress-strain relations attained from coupon testing were used. The comparison of the experimental data recorded from LS-T4 and the analytical model is shown in Figure 4.42.

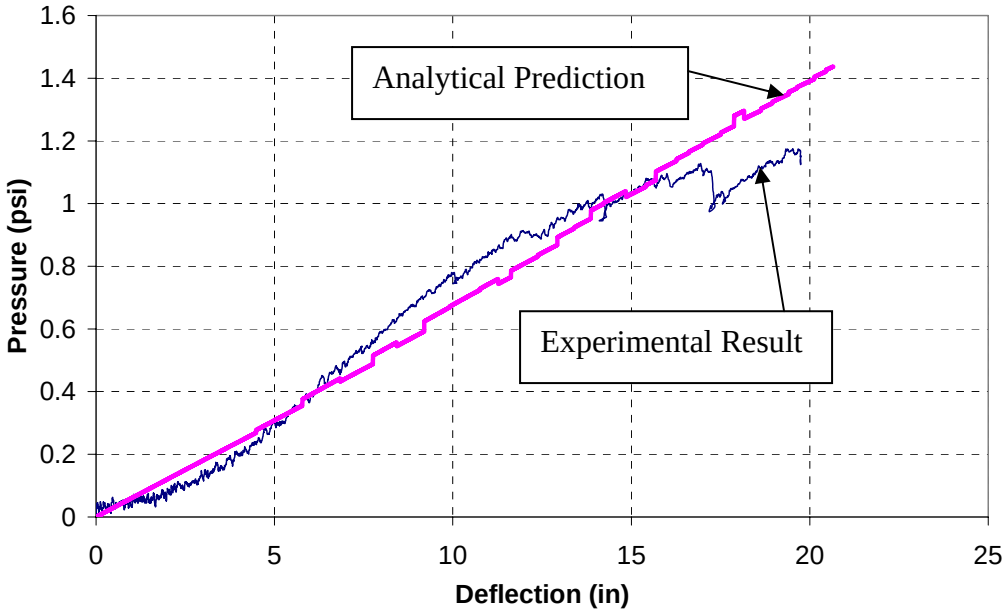

Figure 4.42 - Comparison of Experimental vs. Analytical Data for LS-T4

4.4.4 Summary and Conclusion

From each of the comparisons, it can be seen that the analytical model predicted the behavior of the polymer sheets very well. It can also be seen that increasing the bolt spacing to 16 in. resulted in no energy absorption loss. For this reason, it is recommended to use the 16 in. bolt spacing for design. Additionally, by increasing the thickness of the polymer from 0.125 in. to 0.16 in., it was able to absorb much more energy. However, based on the comparisons, the analytical model predicted the smaller thickness much better than the larger thickness. More testing of thickness should be performed in order to see if this trend continues for thicker polymers.

From the graphs, it can be seen that the model predicts the data very well at low deflections and then becomes less accurate. This can be attributed to a couple of factors,

which includes that the tree's 16 loading points begin to slip at high deflections due to the angle it makes with the polymer sheets and that the loading points become less orthogonal with the polymer.

CHAPTER 5 – DYNAMIC MODELING

5.1 General

The dynamic modeling portion of this report shows how a polymer sheet on a CMU wall behaves under blast loading. It predicts whether or not the system will survive a blast load. There are two primary methods used for dynamic modeling: rigorous methods and numerical analysis. Numerical analysis, that is, solution of the differential equations of motion by arithmetic procedures, is a much more general attack on the problem than rigorous methods because the latter requires the loading and resistance functions to be expressed by relatively simple mathematical terms (Biggs, 1964). Under blast loading, this is very difficult to accomplish. Throughout this chapter, a numerical analysis is used with several approximations to ease the complexity of the design without eliminating the integrity of the design.

Most structures designed today can be idealized with a combination of springs and masses. For example, a simply supported beam with a distributed loading can be idealized as an equivalent single degree of freedom (SDOF) spring mass system shown in Figure 5.1. It is only necessary to formulate proper system parameters such as effective load, F_e, effective mass, M_e, and effective stiffness, k_e. Many of these constants are simply found such as M_e, which is the mass of the total system, and k_e which can be found from material properties of the beam since it is merely a ratio of force to deflection (Biggs, 1964).

For most dynamic modeling, the effects of damping are taken into account. However, the effect may not be significant if the load duration is short and only the maximum dynamic response is of interest (Biggs, 1964). Since blast loads are defined by

high pressures imparted over a very short duration, the effects of damping can be ignored for the dynamic modeling of a structural system under blast loading (Kiger and Salim, 1998).

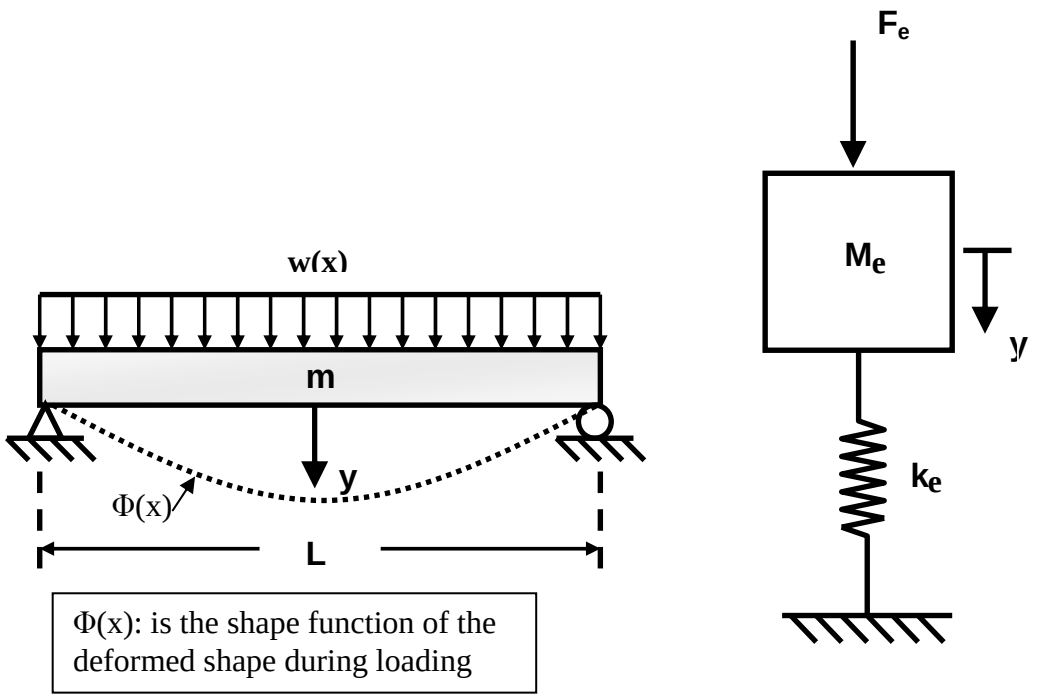

Figure 5.1 – Beam Idealized as SDOF Mass and Spring System

5.2 SDOF Dynamic Modeling

A SDOF is defined to be a system in which only one type of motion is possible and can be defined in terms of a single coordinate. As for this case, the mass in Figure 5.1 can only move in the vertical direction. This is how the polymer sheet is designed for blast loading.

The first step in dynamic modeling is to isolate the mass by drawing a free body diagram (Figure 5.2). To do this, external forces and the spring force, $k_e\, y(t)$, are applied.

Additionally, the inertia force is applied to the mass, which is equal to the mass times the acceleration (Biggs, 1964).

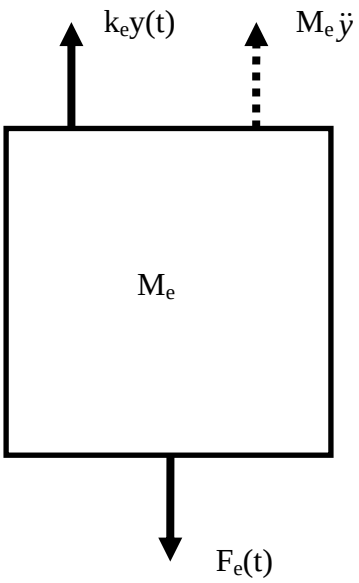

Figure 5.2 – Free Body Diagram (FBD) of the Mass

From equilibrium of the FBD in Figure 5.2, the equation of motion becomes

$$F_e(t) - M_e \ddot{y}(t) - k_e y(t) = 0 \qquad (5.1)$$

Where $k_e\, y(t)$ is the static resistance function which was analytically modeled in Chapter 3.

In order to define an equivalent one degree system, it is necessary to evaluate the parameters of that system, namely, M_e, k_e, and F_e. These parameters come from transformation factors which will be discussed later. Additionally, the load-time function, $F_e(t)$, must be established. A typical blast load is shown in Figure 5.3 which shows how the loading function is idealized. Typically, the negative phase of the loading

function is conservatively ignored. However, it has been found that this region of the loading function reduces the deflection of the wall significantly and should be included. The idealized negative loading region is shown in Figure 5.4. The equivalent system is selected so that the deflection of the concentrated mass is the same as that for some significant point of the structure, such as the mid-point. The constants of the equivalent system are then evaluated on the basis of an assumed shape of the actual structure. This shape is taken to be the same as that resulting from the static application of the dynamic loading (Biggs, 1964).

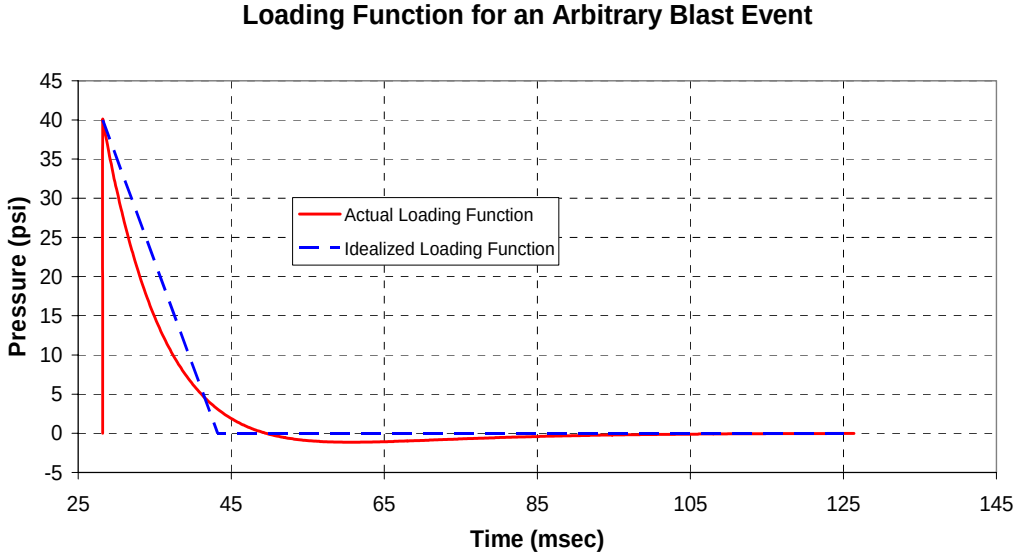

Figure 5.3 – Pressure-time Plot of a Blast Event

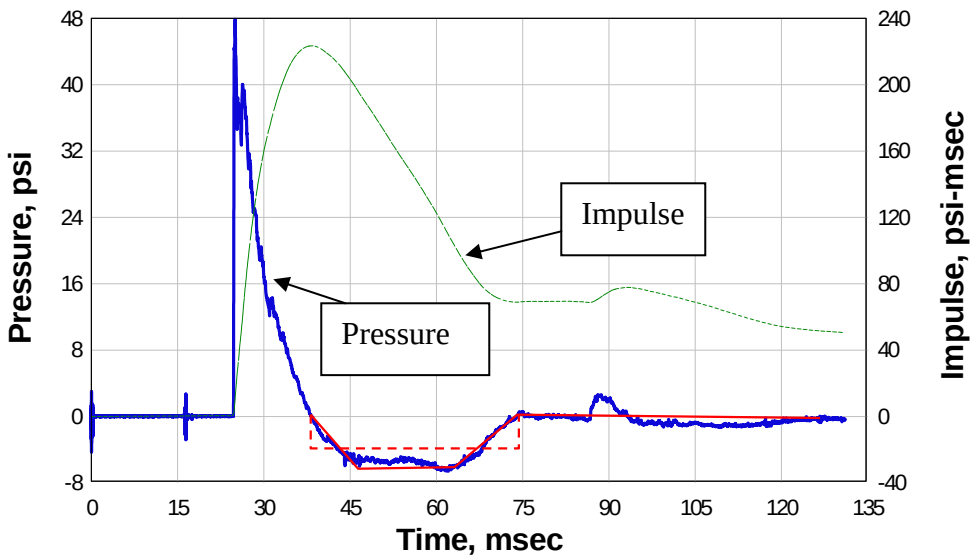

Figure 5.4 – Negative Loading Region Idealized

For convenience, transformation factors, K, are used to convert the real system into the equivalent system. When the total load, mass, resistance, and stiffness of the real structure are multiplied by the corresponding transformation factors, the equivalent one-degree system factors are obtained (Biggs, 1964).

Each of the transformation factors comes from Biggs book *Introduction to Structural Dynamics(1964).* The equivalent mass, M_e, of the equivalent one-degree system for a structure with continuous mass, is given by

$$M_e = \int^{L} m\Phi^2(x)dx \qquad (5.2)$$

Where:

m = mass per unit length
Φ = is the assumed-shape function on which the equivalent system is based

Now the mass factor, K_M, is introduced, which is defined as the ratio of equivalent mass to the actual total mass of the structure.

$$K_M = \frac{M_e}{M_T} \qquad (5.3)$$

For the purpose of this report, the above parameters are:

M_T = mL
L = span of the beam
M_e = given by Equation (5.2)

By substituting these parameters into Equation (5.3), K_M can be written as:

$$K_M = \frac{1}{L}\int^{L} \phi^2(x)dx \qquad (5.4)$$

The equivalent force on the idealized system for a beam with continuously distributed force along the entire length of the beam is given by the equation:

$$F_e = \int^{L} w(x)\phi(x)dx \qquad (5.5)$$

Where:

w(x) = applied distributed load
ø(x) = assumed shape function

The load factor K_L is defined as the ratio of equivalent to actual total force.

$$K_L = \frac{F_e}{F_T} \qquad (5.6)$$

For the beam shown in Figure 5.1, F_T = wL and F_e is given by Equation (5.5).

The resistance of an element is the internal force tending to restore the element to its unloaded static position. Thus, the maximum resistance is the total load having the given distribution which the element could support statically. The stiffness is numerically equal to the total load of the same distribution which would cause a unit deflection at the point where the deflection is equal to that of the equivalent system. Due to this, the resistance factor, K_R, is equal to the load factor, K_L (Biggs, 1964).

$$K_R = \frac{R_{me}}{R_m} = K_L \quad \text{and} \quad K_R = \frac{k_e}{k} = K_L \tag{5.7}$$

Where:

K_L = given by Equation (5.6)
R_m = is the maximum value of wL, or the plastic-limit load which the beam could support statically
R_{me} = same as R_m but for the equivalent system
k = is the value of wL which would cause a unit elastic deflection at mid span

Resistance and deflection are related in the elastic range by R = ky for the real structure and $R_e = k_e y$ for the equivalent system.

The load mass factor, K_{LM}, which is merely the ratio of the mass and load factors can now be used in the equation of motion, which is convenient since the equation can be written in terms of that factor alone. Equation (5.1) can now be written in the form of the real system with equivalent transformation factors:

$$K_{LM} M_T \ddot{y}(t) + ky(t) = F(t) \tag{5.8}$$

Replacing ky(t) with the static resistance function, R(t), the equation becomes:

$$K_{LM} M_T \ddot{y}(t) + R(t) = F(t) \tag{5.9}$$

5.3 Application of Dynamic Modeling

Numerical analysis described in Biggs (1964) can now be used to solve for the y(t) term. In order to find deflection for each incremental time interval, an Excel sheet was designed (Figure 5.5).

Single Degree of Freedom (SDOF) Dynamic Model

Initial Condition	
bxL	144 in^2
Δ_t	0.0001 sec
M_t	0.1166 lb-sec^2/in
KLMe	0.66
KLMp	0.66
F_o	6,480.00 lb
t_f	0.0097778 sec
y_u	35.00

unit width of wall

Max Response	#N/A	in
Time at Max Response	#N/A	sec
Time at Last IntegrationStep	5	sec

Weight of wall per square inch	0.31	psi
peak pressure	45	psi
Impulse	220	psi-msec
Wall Height	12	ft
Initial Resistnce of the wall	1	psi
Negative pressure	-4	psi
F_o negative	-576	
End negative time	0.04	

t (sec)	F(t)	KLM	F(t)/(KLM Mt)	R	R/(KLM Mt)	ÿ	$\ddot{y}\Delta_t^2$	y	t (sec)	Max Limit
0	6480	0.66	84218.18	144	1871.5152	82346.67	0	0	0	35.00
1E-04	6413.7273	0.66	83356.86	144.0000098	1871.5153	81485.34	0	0	1E-04	35.00
2E-04	6347.4545	0.66	82495.54	144.0000098	1871.5153	80624.02	0	0	2E-04	35.00
3E-04	6281.1818	0.66	81634.21	144.0195103	1871.7687	79762.45	0	0	3E-04	35.00
4E-04	6214.9091	0.66	80772.89	144.0585113	1872.2756	78900.62	0	0.01	4E-04	35.00
5E-04	6148.6364	0.66	79911.57	144.0975123	1872.7825	78038.79	0	0.01	5E-04	35.00
6E-04	6082.3636	0.66	79050.25	144.1365133	1873.2894	77176.96	0	0.01	6E-04	35.00
7E-04	6016.0909	0.66	78188.93	144.1755143	1873.7962	76315.13	0	0.02	7E-04	35.00
8E-04	5949.8182	0.66	77327.60	144.2340158	1874.5566	75453.05	0	0.03	8E-04	35.00
9E-04	5883.5455	0.66	76466.28	144.3120178	1875.5703	74590.71	0	0.03	9E-04	35.00

Figure 5.5 – Partial Calculation of the SDOF Model Using Excel

The steps for using the Excel sheet is outlined in Biggs and are as follows. The first step is to input parameters into the tables shown in Figure 5.5 (i.e., area of wall, incremental time step, mass of the wall, K_{LM} factor, peak pressure, impulse of the blast). Once the factors are input, the first incremental time is set to 0. The next parameter, F(t), is calculated at time 0 from a known blast. The parameter R comes from the analytical model predicted in Chapter 3. The acceleration and the deflection are calculated using equations from Biggs (1964).

$$y^{(s+1)} = 2y^s - y^{(s-1)} + \ddot{y}^s(\Delta t)^2 \qquad (5.9)$$

Where:

$y^{(s+1)}$ = Incremental deflection after y^s
y^s = Present deflection
$y^{(s-1)}$ = Incremental step before y^s
$\ddot{y}$ = Acceleration
Δt = Incremental time step

From this equation, it can be seen that in order to calculate deflection $y^{(s+1)}$, the previous deflections, y^s and $y^{(s-1)}$ must be known. Therefore, in order to calculate the deflection at any time step, $y^{(s+1)}$, the following assumptions must be made (Biggs, 1964).

$$y^0 = 0. \qquad \textit{(5.10a)}$$

$$y^1 = \frac{1}{2}\ddot{y}^0(\Delta t)^2 \qquad \textit{(5.10b)}$$

Now $y^{(s-1)}$ is equal to 0 and y^s is equal to y^1. After the first calculation, Equation (5.9) is used for the remainder of the calculations. Additionally, to calculate $\ddot{y}$ the following equation can be used.

$$\ddot{y} = F(t)/(K_{LM}M_t) - R(t)(K_{LM}M_t) \qquad (5.11)$$

Where:

F(t) = Force as a function of time
K_{LM} = Equivalent SDOF factor discussed above
R(t) = Resistances as a function of time
M_t = Total mass of the wall

The calculation is then performed until the maximum deflection is reached.

This prediction gives the deflection versus time of the polymer sheets. The procedure was also implemented into the AFWAC user-friendly PC-code. The opening screen of AFWAC is shown in Figure 5.6.

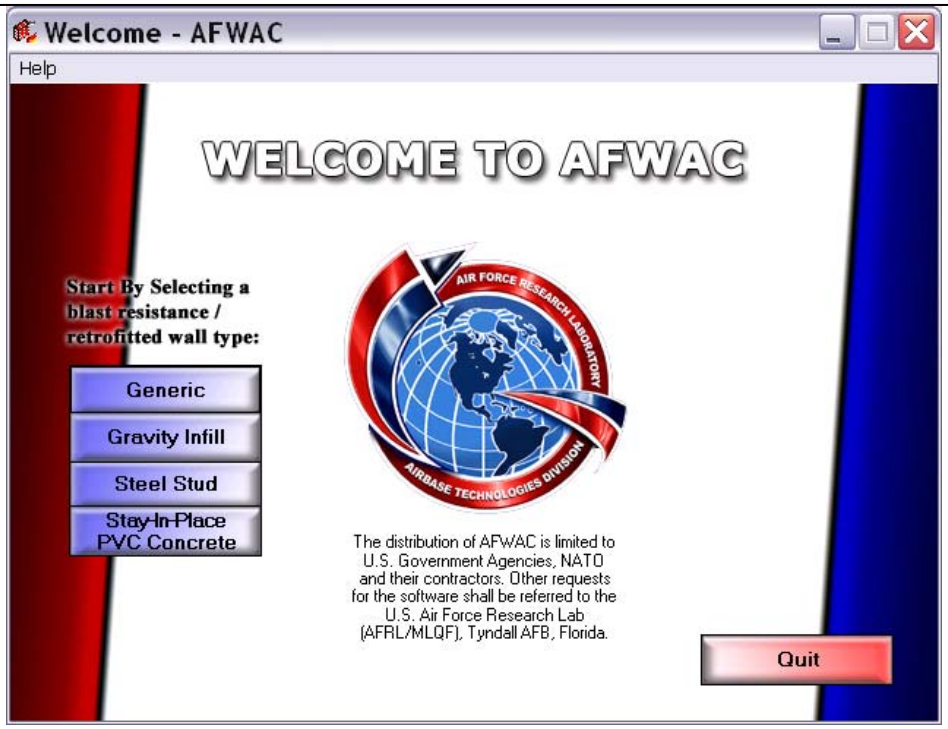

Figure 5.6 – Opening Screen of AFWAC

5.3.1 Effect of CMU Wall Resistance on the Dynamic Response

However, there is additional resistance provided by the CMU wall itself. This resistance depends on the amount of arching that occurs in the wall. The resistance, provided by arching, depends on the gap between the top of the CMU wall and the ceiling. When the shockwave hits the wall, the CMU wall cracks and pushes against the floor and ceiling. If there is a gap between the top of the CMU wall and the ceiling, the CMU wall does not arch until the gap is closed. Since the walls that are being retrofitted are non-load bearing infill CMU walls, there is typically a 1 in. gap between the CMU wall and the ceiling. This gap causes the delayed arching effect, which reduces the resistance of the wall. From the Wall Analysis Code (WAC) prepared by the United

States Army Corps of Engineers Research and Development Center, this procedure was done on a CMU wall without reinforcement. The findings are shown in Figure 5.7.

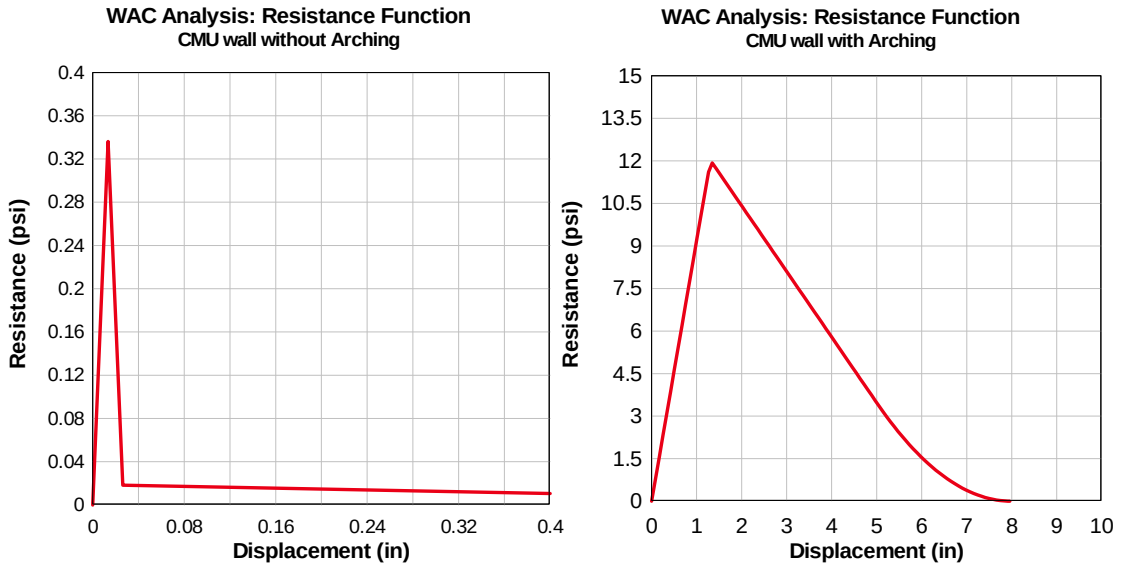

Figure 5.7 – Resistance of a CMU Wall with and without Arching

From Figure 5.7 it can be seen that an unreinforced CMU wall provides a maximum resistance of 0.34 psi without arching but 12 psi resistance with arching. Because of this, a series of plots were made varying the amount of resistance this type of CMU wall provided (Figure 5.8). From the plots, it can be seen that picking a specific resistance can make a large difference in the response of the CMU wall. Based on experimental testing and knowledge from blast design experts, a value of 1 psi was used for the resistance of the CMU wall.

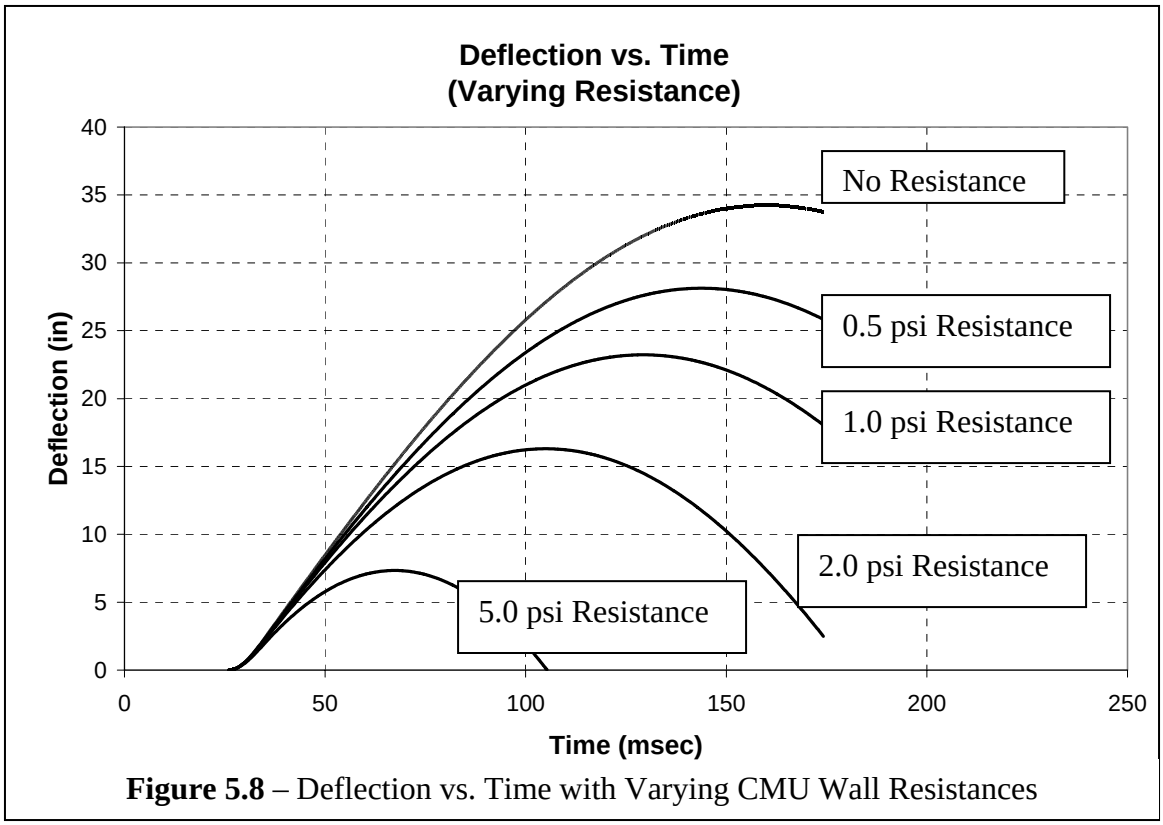

Figure 5.8 – Deflection vs. Time with Varying CMU Wall Resistances

5.3.2 Effect of the Negative Phase on the Dynamic Response

Once the resistance of the wall and the polymer are found, the loading function must be analyzed. A typical blast loading has a positive and a negative region (Figure 5.3). Typically, the negative region is conservatively ignored. However, if the negative region is taken into account, it can provide significant resistance to the initial positive load. A graph was made comparing the effects of the negative loading region of a blast and is shown in Figure 5.9. From the graph it can be seen that by using the negative loading region, the maximum deflection is reduced by 11 in.

The predicted resistance was compared to field testing done at AFRL to verify these results. The resistance function was predicted using an assumed initial resistance of the CMU wall, and the negative phase of the loading was not ignored.

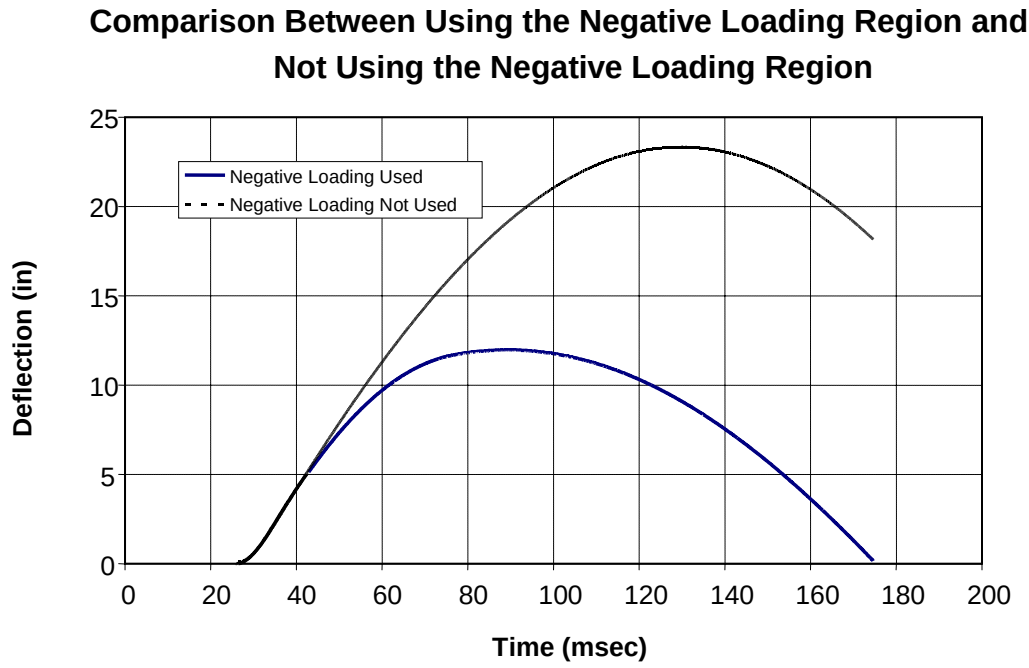

Figure 5.9 – Effects of the Negative Phase on Wall Response

5.4 Field Testing

Several walls have been tested using live explosions for various retrofit systems. As stated in Chapter 2, many retrofit systems such as steel studs, steel sheathing, and several different types of polymers have been tested under blast loading. In this section, the behavior of three polymers were predicted using the procedure outlined in this report and compared to the experimental data received by AFRL. The first polymer, hereafter referred to as P1, is the same sheet polymer analyzed in Chapters 3 and 4. The second polymer, hereafter referred to as P2, is another sheet polymer tested by AFRL in a retrofitted system. The third polymer, hereafter referred to as P3, was tested by AFRL along with P2. P1 and P2 are included to show that the procedure outlined in this report can be used for other types of polymers.

5.4.1 P1 Polymer Sheets

In this section, the P1 polymer sheets analyzed in the previous Chapters are compared with the results of AFRL full-scale test data. Test setups, pre- and posttest photos, and predictions of the wall's behavior are also presented.

5.4.1.1 Test Setup

P1 polymer sheets were anchored behind a typical CMU wall. A 6 x 1/4-in. connection plate braced down with 3/8-in. flat head cap screws spaced approximately every 12 in. (Figure 5.10) were used. An undisclosed explosive was placed a certain distance away from the target to load the retrofitted system. Pressure gages were place around and on the exterior side of the wall along with a deflection gage to measure the displacement at the middle of the wall.

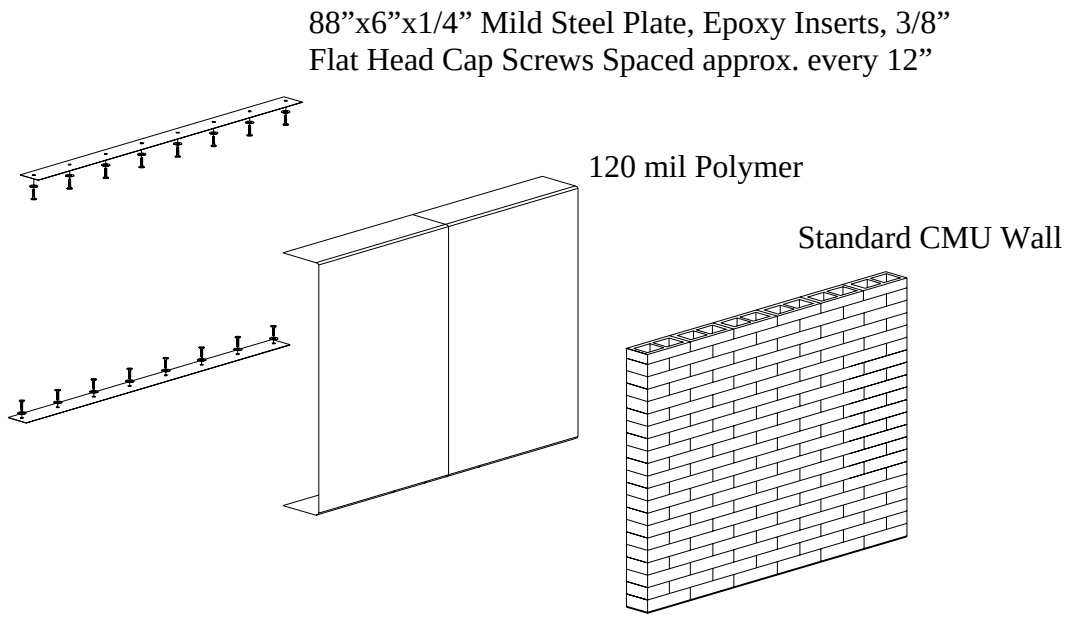

Figure 5.10 – Schematic of the CMU Wall with Polymer Sheet Retrofit

Photos were taken before and after the wall was loaded. Figure 5.11 shows the CMU wall with and without the polymer retrofit. From this figure, the connection plate used to connect the polymer to the floor and ceiling can be seen. Figure 5.11 also shows the device that measured midpoint deflection.

Figure 5.11 – CMU Wall with and without P1 Retrofit

Figure 5.12 depicts the exterior and interior of the wall after the explosion and shows that the polymer retrofit remained intact. Although some of the CMU blocks fell from the wall, none of the fragmentation entered the protected interior space. From these figures, it can be seen that the retrofitted wall is capable of withstanding a blast load produced by a typical explosive threat.

Figure 5.12 – Exterior and Interior of Wall after Explosion

5.4.1.2 Results

For P1, the analytical model that was developed in this report was used in the SDOF which was then used to compare to the experimental results. The analytical model is shown in Figure 5.13a, which was developed using the material response shown in Figure 5.13b for a representative coupon result.

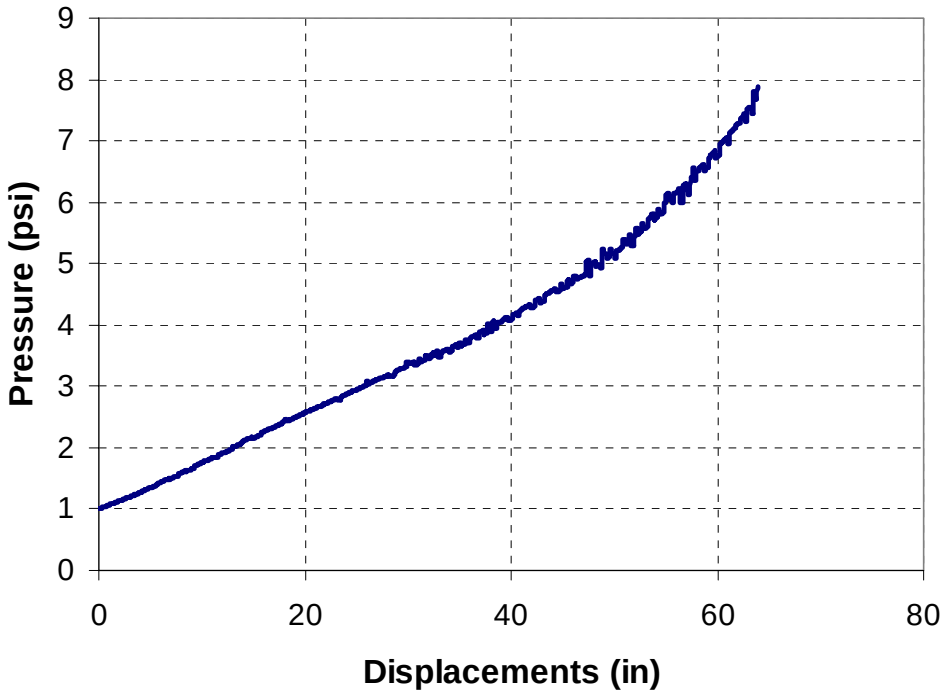

Figure 5.13a – Analytical Model of the Static Resistance Function

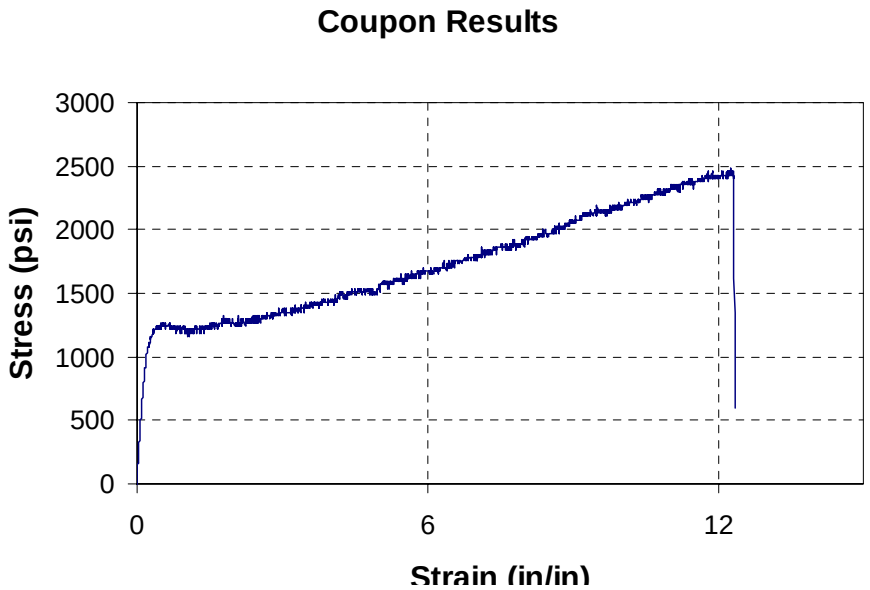

Figure 5.13b – Stress-Strain Relationship for P1

Three gages, R2, R3, and R4, were used to measure the pressure of the blast event. The pressures for each gage were recorded, impulses were calculated, and plots versus time were constructed (Figure 5.14-5.16). The pressures and impulses were averaged and used for the input in the SDOF. Additionally, a deflection gage positioned at the mid-span of the CMU wall was used to make a graph of deflection versus time. The actual deflection versus time graph was compared to the predicted SDOF model of the wall, and results are shown in Figure 5.17. The results show an almost perfect match concluding that the SDOF predicted the response of the wall very well. There is approximately 12% error, which can be attributed to the lack of information on the contribution of arching to the resistance of the CMU wall. The boundary conditions, including the space between the top of the wall and ceiling, were not known.

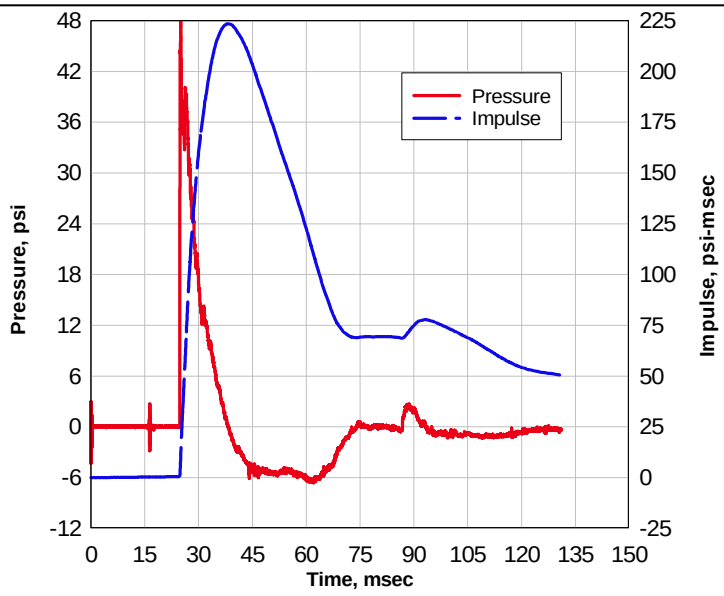

Figure 5.14 – Pressure and Impulse vs. Time for Gage R2

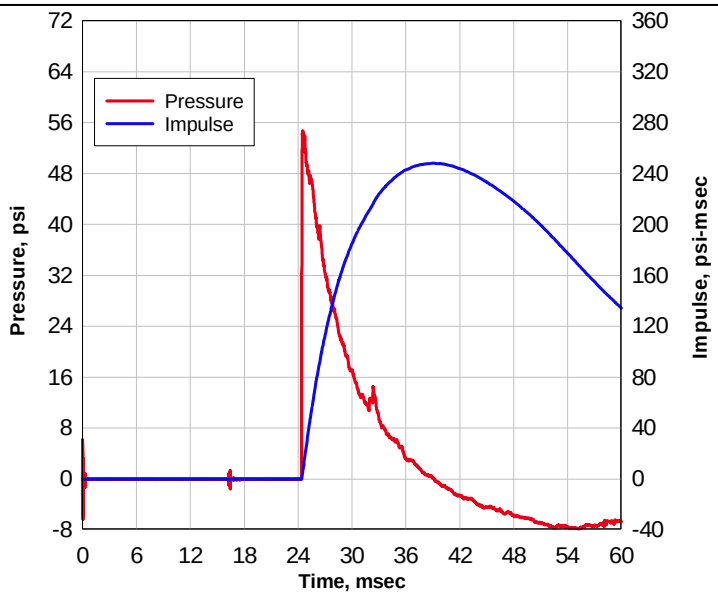

Figure 5.15 – Pressure and Impulse vs. Time for Gage R3

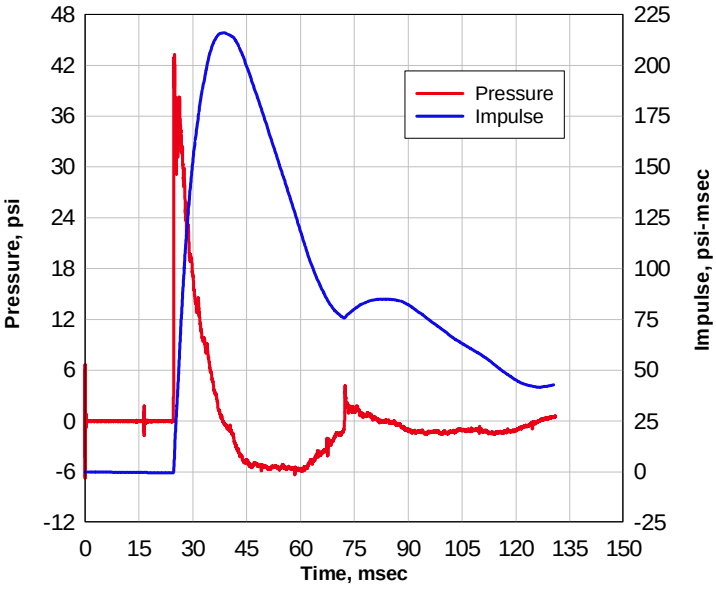

Figure 5.16 – Pressure and Impulse vs. Time for Gage R4

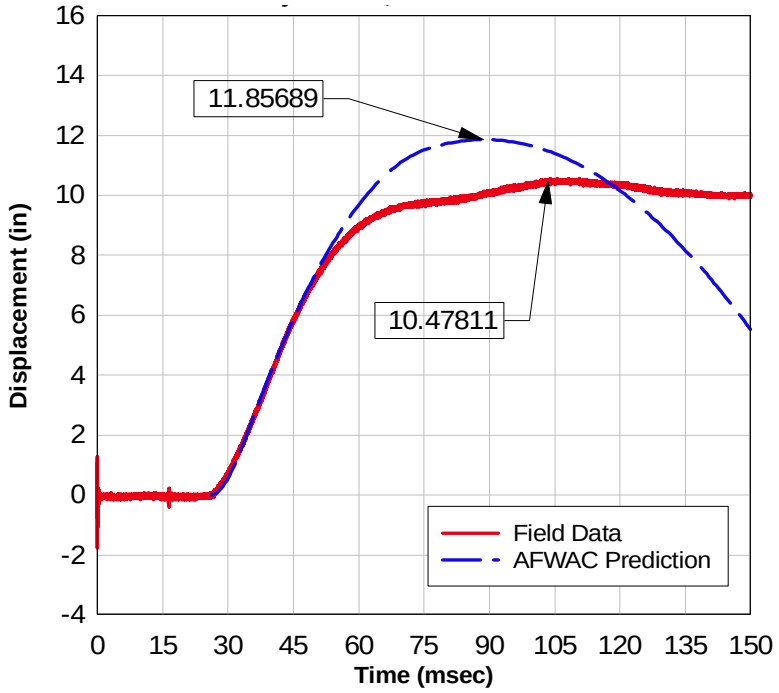

Figure 5.17 – Comparison of the Predicted SDOF Model to Actual Response of P1 Retrofit

5.4.2 P2 Polymer Sheets

P2 sheets were also tested by AFRL. In this section, an analytical model was predicted as shown in Chapter 3, and then this was used to develop a SDOF model as shown in Chapter 5. Finally, the results of this SDOF model were compared to the findings from the live testing.

5.4.2.1 Test Setup

Polymer P2 was anchored behind a typical CMU wall. A 6 x 1/4-in. connection plate braced down with 3/8-in. flat head cap screws spaced approximately every 12 in. was used. An undisclosed explosive was placed a certain distance away from the target to load the retrofitted system. Pressure gages were place around and on the exterior side

of the wall along with a deflection gage to measure the displacement at the middle of the wall. For comparisons, the middle reflected pressure gage was used.

Before the test, photos were taken of the test setup. Figure 5.18 shows the P2 polymer on the interior side of the CMU wall. Also shown is the device used to measure the deflection of the wall. Figure 5.19 depicts how the P2 polymer was connected to the floor and ceiling.

Additionally, photos were taken after the test was conducted. Figure 5.20 shows the exterior of the CMU wall after the test. The wall on the left was retrofitted with the P2 polymer retrofit.

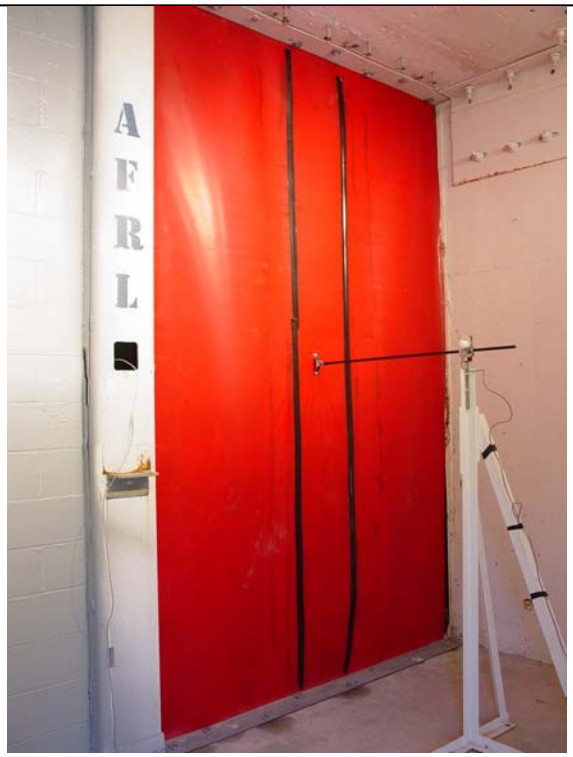

Figure 5.18 – CMU Wall with P2 Polymer Retrofit

Figure 5.19 – P2 Polymer Floor Connection

Figure 5.20 – Exterior of CMU Wall after Explosion

5.4.2.2 Prediction

The same procedure was used to develop a SDOF to compare with the experimental results. First, coupon tests were conducted to find the relationship between stress and strain. Figure 5.21 shows the coupon being stretched. Figure 5.22 shows the typical relationship between stress and strain from the coupon testing. Once this was known, an analytical model (Static Resistance Function) was developed for the SDOF. The analytical model is shown in Figure 5.23. Then, the SDOF model was developed, and a comparison was made between the experimental and predicted results.

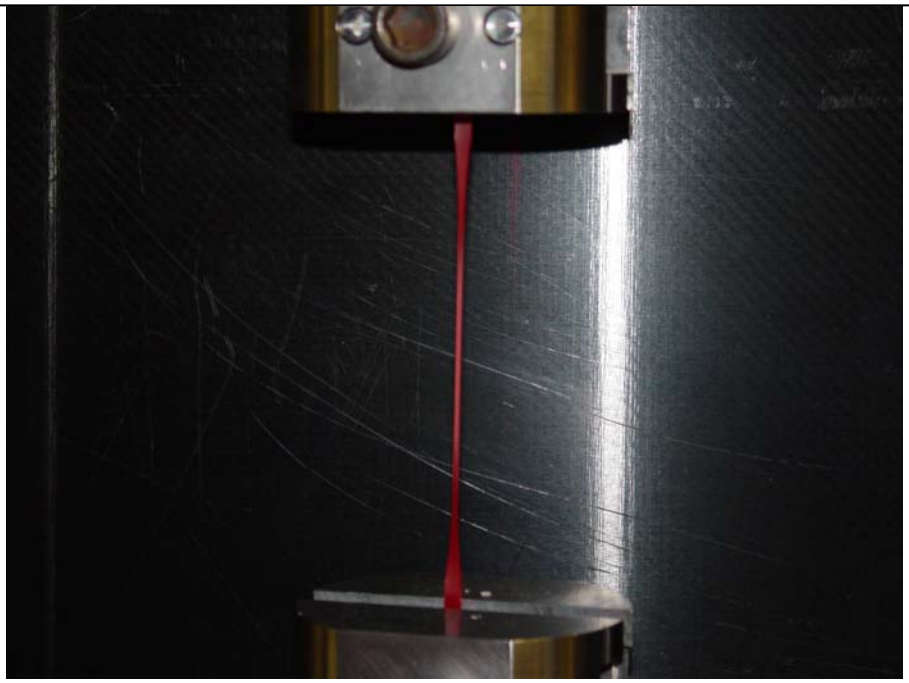

Figure 5.21 – Coupon Testing of a P2 Sample

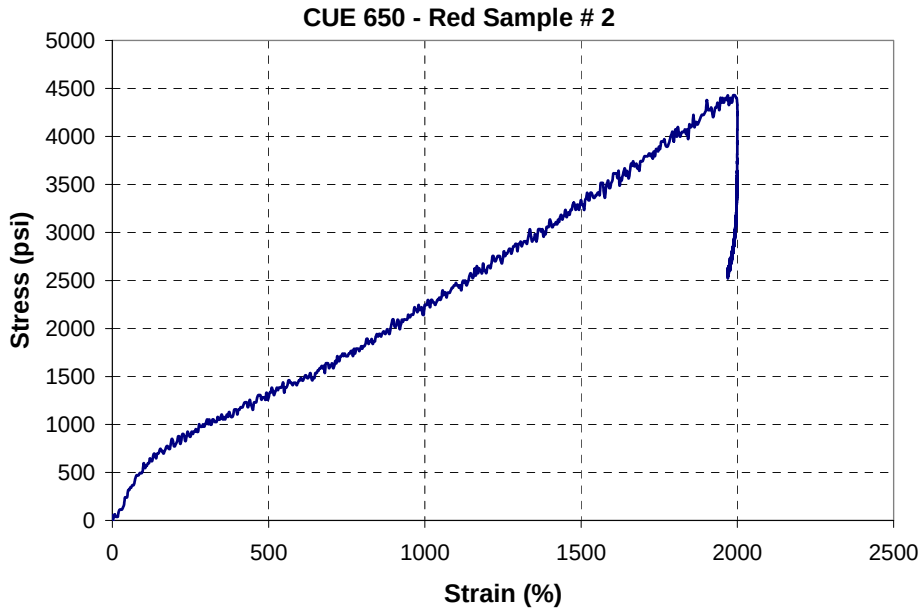

Figure 5.22 – Coupon Results of a Typical P2 Sample

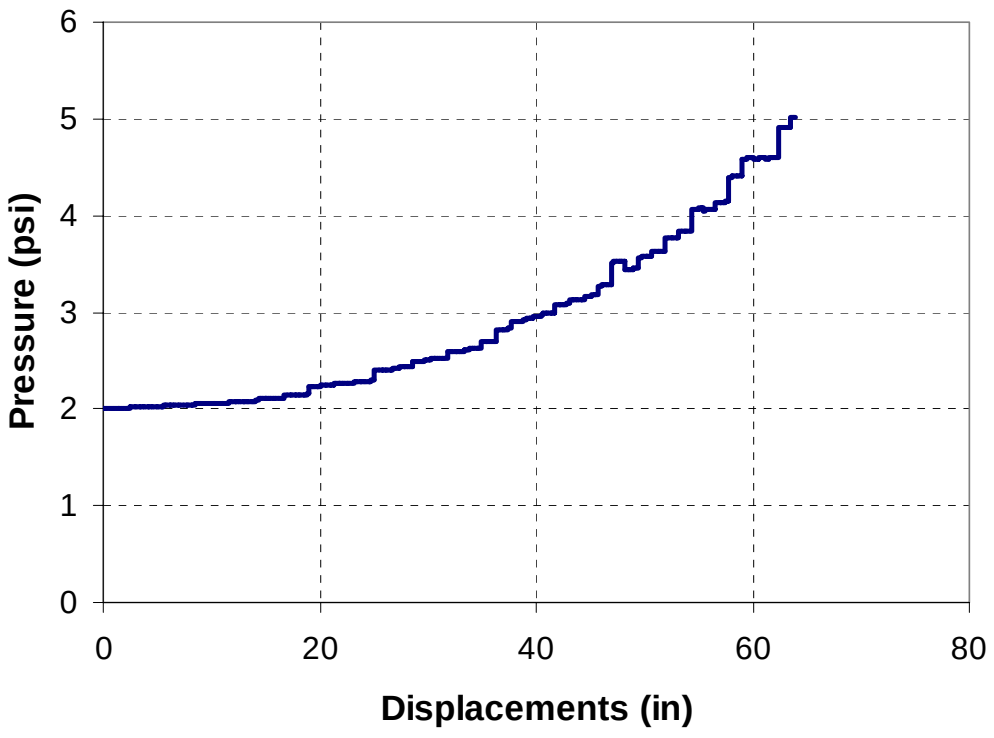

Figure 5.23 – Analytical Model of the P2 Polymer Sheet

5.4.2.3 Results

The reflected pressure gage that was located just to the right of the wall was used as the loading function for the SDOF (Figure 5.24). The SDOF and the experimental results were compared using a CMU wall resistance of 2 psi. It should be noted that the resistance provide by the CMU wall itself varies greatly with the amount of arching that occurs. It is recommended that further testing be conducted on this topic. The prediction and the actual results were compared and are shown in Figure 5.25. From the graph, it can be seen that the predicted model lines up quite well with the actual experimental results. There is approximately 18% error, which can also be attributed to the effect of unknown boundary conditions on the resistance of the CMU wall.

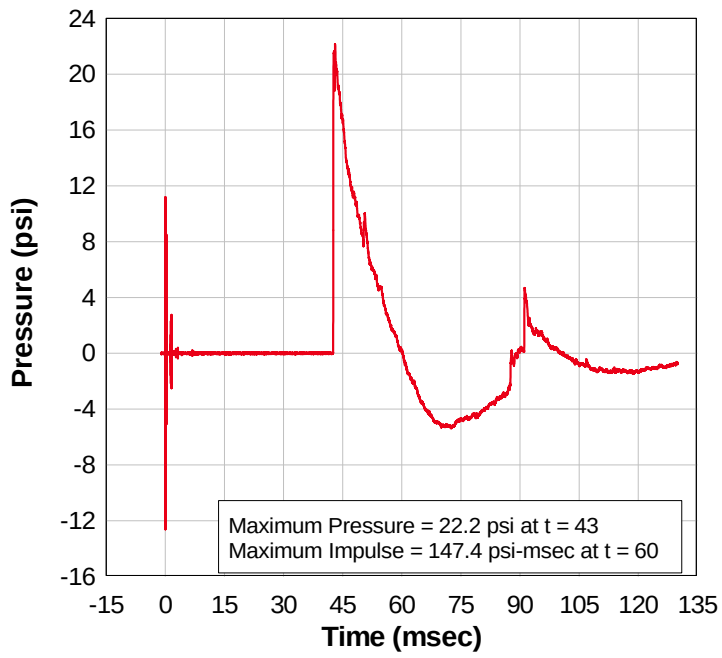

Figure 5.24 – Loading Function from the Pressure Gage for the P2 Wall

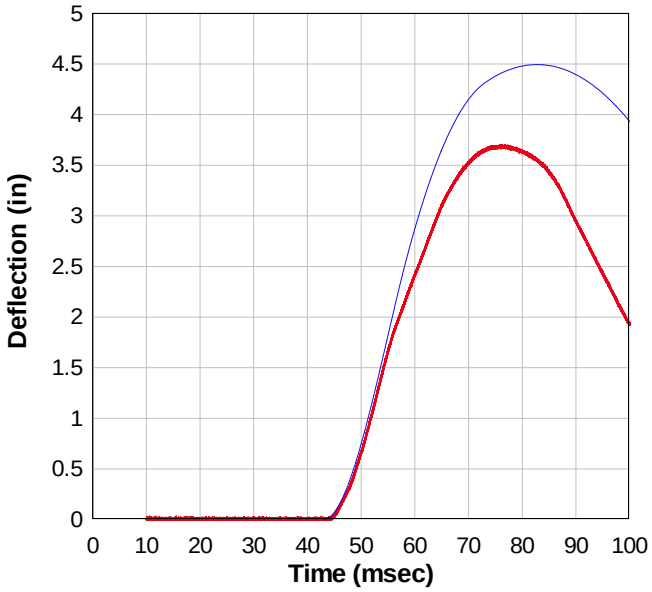

Figure 5.25 – Comparison of the Predicted SDOF Model to Actual Response of P2 Retrofit

5.4.3 P3 Polymer

The P3 polymer was also tested by AFRL. In this section, an analytical model was predicted as shown in Chapter 3, and then this was used to develop a SDOF model as shown in Chapter 5. Finally, the results of this SDOF model were compared to the response of the wall measured during live testing.

5.4.3.1 Test Setup

Polymer P3 was sprayed on a typical CMU wall approximately 0.125 in. thick. The polymer was sprayed over the wall and extended up to 12 in. along the floor and ceiling of the reaction structure. No mechanical connections were used to connect the polymer to the ceiling and floor, instead the bond between the polymer and ceiling/floor was used to provide the necessary anchorage. An undisclosed explosive was placed a

certain distance away from the target to load the retrofitted system. Pressure gages were placed around and on the exterior side of the wall, and a deflection gage measured the displacement at the middle of the wall. For comparisons, the middle reflected pressure gage was used.

Photos were taken prior to the test setup. Figure 5.26 shows the P3 polymer on the interior side of the CMU wall. Also shown is the device used to measure the deflection of the wall. Photos were also taken after the test was conducted. Figure 5.27 shows the exterior side of the CMU wall after the test.

Figure 5.26 – CMU Wall with P3 Polymer Retrofit

Figure 5.27 – CMU Wall Retrofitted with P3 Polymer after Explosion

5.4.3.2 Prediction

The same procedure was used to develop a SDOF model to compare with the experimental results. First, coupon tests were conducted to find the relationship between stress and strain. Figure 5.28 shows the relationship between stress and strain from a typical coupon test. Once this was known, an analytical model (Static Resistance Function) was developed for the SDOF model. The analytical model is shown in Figure 5.29. Then, the SDOF was developed, and a comparison was made between the experimental and predicted results.

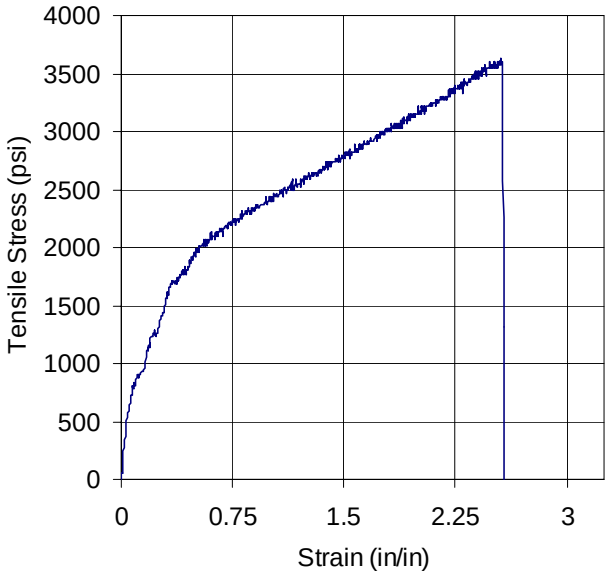

Figure 5.28 – Typical Coupon Results of P3 Polymer

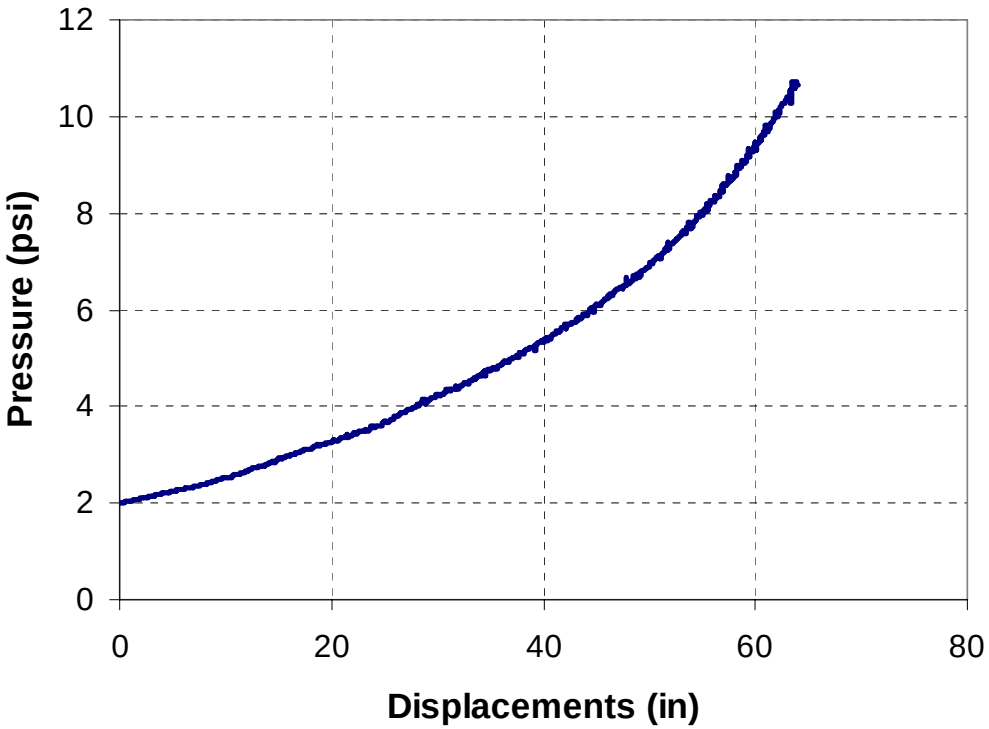

Figure 5.29 – Analytical Model of P3 Retrofit System

5.4.3.3 Results

The reflected pressure gage that was located just to the right of the wall was used as the loading function for the SDOF (Figure 5.30). The SDOF and the experimental results were compared using a CMU wall resistance of 2 psi. As stated above, this is arbitrary and should be researched further. The prediction and the actual results were compared and are shown in Figure 5.31. From the graph, it can be seen that the predicted model lines up quite well with the measured response. There is approximately 18% error, which can also be attributed to the effect of unknown boundary conditions on the resistance of the CMU wall.

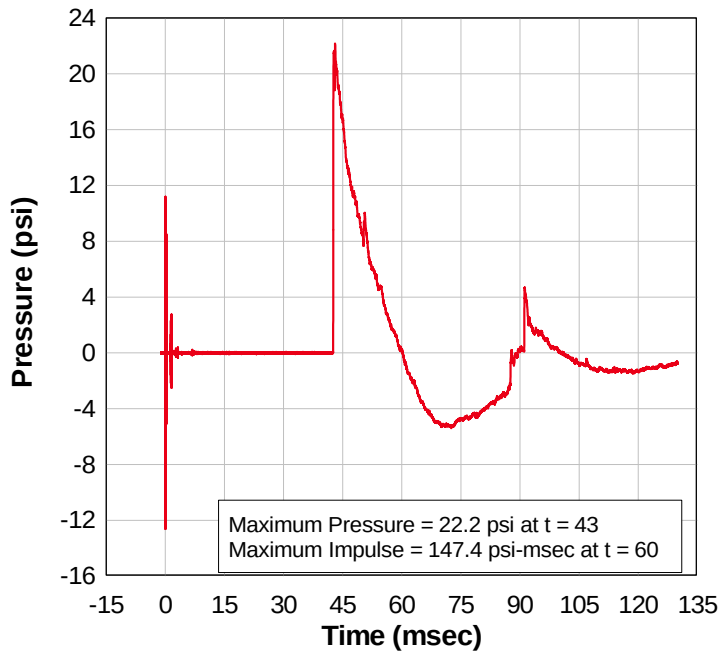

Figure 5.30 – Loading Function from the Reflected Pressure Gage

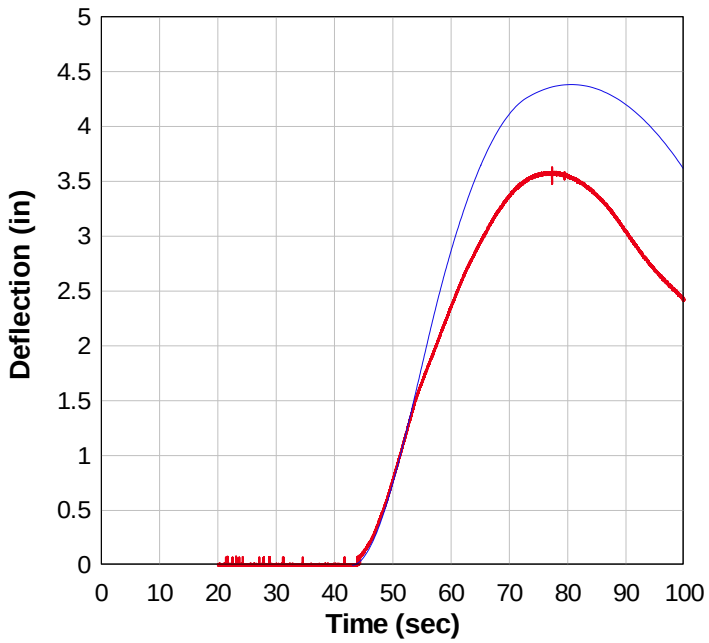

Figure 5.31 – Comparison of the Predicted SDOF Model to Actual Response of P3 Retrofit

5.5 Summary and Conclusions

SDOF dynamic modeling is very useful in idealizing a complicated structure into an equivalent model with simple analysis. All of the predictions model the behavior of the retrofitted system very well based on some assumptions regarding the resistance of the CMU walls. The research developed in this report has been implemented into the computer code AFWAC which will be used to design blast retrofitted walls using polymers. Additionally, dynamic modeling has shown that these polymers are an efficient way to retrofit CMU walls. They limit the amount of debris that is projected into the interior of a building and provide sufficient strength to ensure the wall will not also collapse on the occupants.

CHAPTER 6 – CONCLUSIONS AND RECOMMENDATIONS

In this report, an analytical model verified by experimental data was used to develop engineering design methodology for blast-retrofit of CMU walls using polymer sheets. The results were then implemented into the computer program AFWAC. This research found that polymer sheets provide stability and ample ductility to CMU walls during a blast loading event.

- From the coupon tests, it was found that the polymer sheets have the ability to provide enormous amounts of energy absorption capabilities if allowed to develop to their full capacity.
- From the connection tests, it was found that to utilize the polymers full energy absorption capabilities, a 6 x 1/4-in. connection plate and bolt spacing of 12 or 16 in. should be used.
- As the thickness of the polymer increased, the accuracy of the analytical prediction decreased. Since there were only two thicknesses tested and four tests conducted, further research should be conducted to explore more samples with variable thicknesses.
- Both the 16 in. and 12 in. bolt spacings performed the same in the component testing portion. The 16 in. bolt spacing is recommended for the use in design practices of the polymer sheets used in this report.
- Both the 0.125 in. and 0.16 in. polymer thicknesses provide adequate ductility for the use in retrofit design.

- Through live testing, the polymer sheets showed that they provided adequate resistance to blast loading. Additionally, the polymer sheets limited the amount of debris that entered into the interior space and provided adequate resistance to collapse of the walls. Polymer sheets proved to be a good material to retrofit CMU walls for blast design.
- It was found that the resistance of the CMU wall has a significant effect on the response of the CMU-polymer wall retrofit system. It is recommended that more testing be completed to find a more accurate CMU wall resistance based on the boundary conditions.
- The negative phase of the blast loading was found to significantly affect the predicted response of the wall system. Therefore, it is also recommended that the negative phase be incorporated into the design of the CMU wall retrofit with polymer sheets.
- The failure of the CMU-polymer wall system could be controlled by ductility limits of the polymer and/or by tear strength due to localized stress concentrations areas at the edge of the clamping plate or at mortar joints. Therefore, it is recommended that additional research be conducted to develop predictive models of failure limit states that can be included into AFWAC.
- Little is known what long-term effects wear and erosion will have on the polymers especially for the spray-on polymer since the bond between the polymer and the CMU wall may decrease. Further testing should be completed on this subject.

REFERENCES

AFWAC (2005). Air Force Wall Analysis Code. Preliminary version developed by the University of Missouri-Columbia for the Air Force Research Laboratory, Version 1.1. December 2005.

Albert, M. (2001). "Strengthening of Unreinforced Masonry Walls Using FRPs." *Journal of Composites for Construction.* American Society of Civil Engineers. Paper No. 21441. Reston, VA.

Beckman, S. (2005). "Evaluation of Polymer Retrofit of CMU Walls for Blast Protection." Honors Thesis, University of Missouri-Columbia, Department of Civil and Environmental Engineering, Columbia, MO 65211-2200.

Bechtold, J. (2004). "Evaluation of Polymer Retrofit Systems for Concrete Masonry Unit (CMU) Wall Systems: Evaluation of the Concrete-Polymer Interaction." Honors Thesis, University of Missouri-Columbia, Department of Civil and Environmental Engineering, Columbia, MO 65211-2200.

Biggs, J. M. (1964). *Introduction to Structural Dynamics*. McGraw-Hill, Inc., New York.

Davidson, J. (2004). "Explosive Testing of Polymer Retrofit Masonry Walls." *Journal of Performance of Constructed Facilities.* American Society of Civil Engineers. Vol. 18, Number 2, pp 100-106. Reston, VA.

Davidson, J. (2005). "Failure Mechanisms of Polymer-Reinforced Concrete Masonry Walls Subjected to Blast." *Journal of Structural Engineering.* American Society of Civil Engineers. Vol. 131, Number 8, pp 1194-1205. Reston, VA.

Dinan, R. (2005). "Blast Resistant Steel Stud Wall Design." Doctoral Dissertation, University of Missouri, Department of Civil Engineering, Columbia, MO 65211-2200.

Hilti (2001). *Systems and Solutions Customer Catalogue* [Brochure]. Tulsa, OK.

Kennedy, J. (2005). "Analytical and Experimental Evaluation of Steel Sheets for Blast Retrofit Design." Masters Thesis, University of Missouri-Columbia, Department of Civil Engineering, Columbia, MO, 65211-2200

Lane, J. (2003). "Modeling and Design of Explosion Resistant Steel Stud Wall Systems." Masters Thesis, University of Missouri, Department of Civil Engineering, Columbia, MO, 65211-2200.

Kiger, S. and Salim, H. (1998). "Use and Misuse of Structural Damping in Blast Response Calculations." Concrete and Blast Effects, ACI Special Publication SP-175, pp.121-130.

Stone, H. and Engebretsen, J. "The Basics of Blast Resistant Design." Proc. 70th Annual Convention, Structural Engineers Association of California. pp. 87-94.